

Permian paleomagnetism of the Tien Shan fold belt, Central Asia: post-collisional rotations and deformation

Mikhail L. Bazhenov^{a,*}, Valentin S. Burtman^a, Ariadna V. Dvorova^a

^a *Geological Institute, Russian Academy of Sciences, Moscow, Russia*

Received 30 June 1998; accepted 25 May 1999

Abstract

Permian volcanic and sedimentary rocks were sampled from eight localities in the western and central parts of the Tien Shan fold belt. High-temperature, sometimes intermediate-temperature components isolated from these rocks at seven localities after stepwise thermal demagnetization are shown either to predate folding or be acquired during deformation; the conglomerate test at some localities is positive. The observed inclinations fit rather well with the Eurasian reference data, whereas the declinations are strongly deflected westward; westerly declinations have already been observed from the other parts of the Tien Shan (from the Turan plate in the west to the northern rim of Tarim and the Urumque area in the east). Our analysis shows that a considerable counterclockwise rotation of the Tien Shan fold belt as a rigid body is geologically improbable. We hypothesize that a sinistral shear zone existed over the fold belt thus accounting for systematically westerly declinations. This zone is about 300 km wide and is traced along the Tien Shan fold belt for 2500 km. A large area of Permian alkali magmatism in the West and Central Tien Shan is interpreted as an extensional domain conjugated with the shear zone. This shear zone can be accounted for by translation of the Kara Kum and Tarim blocks along the Eurasian boundary after their oblique collision in the Late Carboniferous. Two phases of rotation are recognized in the Tien Shan. The earlier rotation took place under shear strain during the D3 stage of deformation in the Artinskian–Ufimian. The later rotation is connected with transpression (D4 stage of deformation) and could occur from the Late Permian to Early Jurassic. © 1999 Elsevier Science B.V. All rights reserved.

Keywords: paleomagnetism; tectonics; Central Asia; late Paleozoic; shear zone

1. Introduction

Eurasia is certainly the largest and likely the most tectonically heterogeneous of the continents. While other continents comprise a Precambrian nucleus bordered by fold belts of various ages, Eurasia consists of several ancient blocks whose amalgamation into a composite continent encompasses the entire Phanerozoic. The East European, Siberian, Tarim

and other platforms and numerous smaller blocks were widely separated during most of the Paleozoic and welded together by its end, resulting in the formation of the huge Ural–Mongol fold belt. This fold belt stretches from the northern Urals through Kazakhstan and south Siberia almost to the Pacific. Thus our understanding of Asian tectonics largely depends on deciphering the Ural–Mongol fold belt evolution.

The south-central part of the Ural–Mongol fold belt, the Tien-Shan, stretches for about 2500 km from Inner Mongolia in the east to the Turan plate

* Corresponding author. E-mail: palmag@glas.apc.org

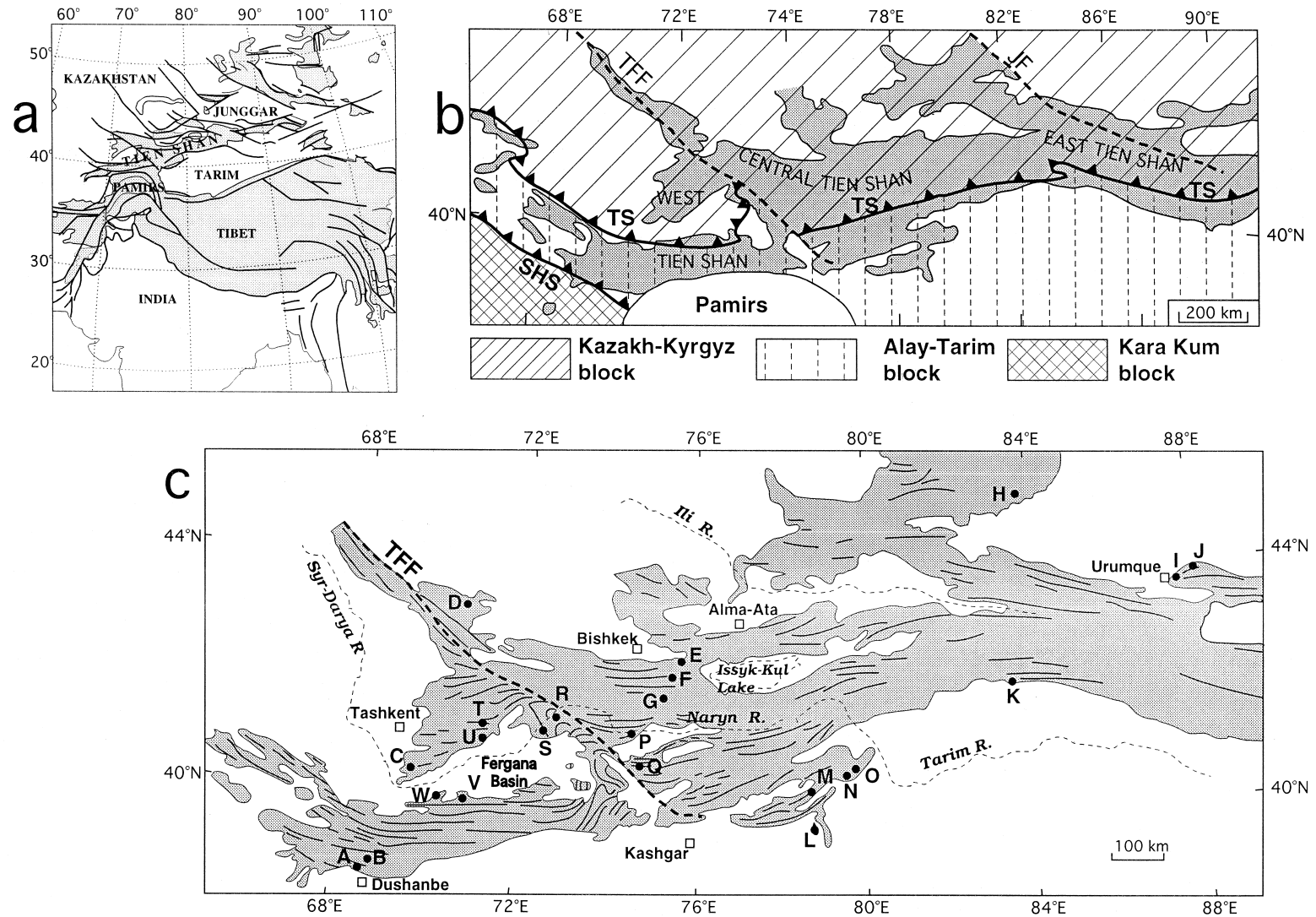


Fig. 1. General location map showing major faults and areas with elevations greater than 2 km (shaded) simplified after Cobbold and Davy (1988). (b) Paleozoic sialic blocks in the modern structure of the Tien Shan. Paleozoic rocks are shaded. Thick toothed lines are main sutures: *TS* = Turkestan suture, *SHS* = South Hissar suture. Thick dashed lines are main strike-slip faults: *TFF* = Talas–Fergana Fault, *JF* = Junggar Fault. (c) The axes of late Paleozoic folds in the Tien Shan (shaded) and paleomagnetic sampling localities (dots): *A–O*, the localities labeled as in Bazhenov et al. (1993); *P–W*, this study.

in the west, and is divided into the West, Central and East Tien Shan (Fig. 1a,b). The Tien Shan fold belt resulted from the late Paleozoic collision of the Kazakh–Kyrgyz, Alay–Tarim and Kara Kum continental blocks (Burtman, 1980, 1997). Until the Late Carboniferous, the Kazakh–Kyrgyz and Alay–Tarim blocks were separated by the Turkestan Ocean, whereas the South Hissar branch of the Paleotethys divided the Alay–Tarim and Kara Kum blocks. All blocks have a Precambrian basement which locally outcrops among folded Paleozoic rocks (Akhmetjanov et al., 1982). In the southern part of the Alay–Tarim block (Tarim zone), the basement is coated by a Paleozoic platform cover, while the Alay zone in the north consists of deformed sediments of Paleozoic shelf and continental slope of the Turkestan Ocean. The Alay–Tarim and Kara Kum block probably existed as separate units since the Late Precambrian (Bakirov et al., 1984). The composite Kazakh–Kyrgyz block resulted from amalgamation of early Paleozoic island arcs after the closure of inter-arc basins in the Ordovician (Burtman, 1997).

The Kyrgyz (northern in the present-day coordinates) margin of the Turkestan Ocean was active from the Ordovician until the Early Devonian, passive or transform in the Middle and Late Devonian and most of the Early Carboniferous, and active again in the Serpukhovian time and Late Carboniferous. The southern Alay margin was permanently passive (Burtman, 1997). The Turkestan Ocean was closed in the Moscovian of the Late Carboniferous, and small remnant deep-water basins existed close to the ocean suture until the Early Permian (Biske, 1995). Early Paleozoic evolution of the South Hissar oceanic basin is not documented, both its margins were passive in the middle Paleozoic, and the basin was closed in the Late Carboniferous, the subduction taking place under its northern margin. The South Hissar oceanic basin was closed probably somewhat later than the Turkestan Ocean. As a result, the Tien Shan together with Tarim was welded to Eurasia. The collision led to mountain building, accumulation of continental molasses in the Late Carboniferous and Permian and collisional volcanism characterized by abundant acid lava and intrusions.

The interaction of the collided blocks was long and complex as evidenced by multi-phase late Paleozoic deformation of the Tien Shan (Burtman, 1980,

1984). Many details of this deformation, the mode and magnitude of horizontal movements in particular, are still poorly understood. In addition, this fold belt was re-activated and additionally deformed in the late Cenozoic as the result of the India–Eurasia collision (Molnar and Tapponnier, 1975), and the younger movements have disguised the late Paleozoic structural pattern. Therefore, one has to remove the Cenozoic tectonic ‘overprints’ to evaluate the late Paleozoic evolution of the Tien Shan.

Extensive geological studies have been carried out over the entire Tien Shan, but many characteristics of its geodynamics are still unclear. Some problems may be solved with the aid of paleomagnetic data. While paleomagnetic data from the Chinese Tien Shan are rather recent and were obtained according to modern standards, many results from the West Tien Shan are decades old and are based on blanket cleaning at low to moderate temperatures and/or alternating fields without principal component analysis. These older data often fail in paleomagnetic field tests, the fold test in particular, and their tectonic significance is ambiguous.

In this article, we present new Permian paleomagnetic results from different parts of the West and Central Tien Shan (localities P–W, Fig. 1b,c). We also analyze the spatial distribution of Permian alkali magmatism and available paleomagnetic data all over the Tien Shan and present a scenario of geodynamic evolution of this belt since the late Paleozoic.

2. Sampling

Clastic rocks, often red beds, shallow-marine deposits and subaerial volcanics started accumulating in the Tien Shan belt in the Late Carboniferous and Permian. Only small deep-water basins filled with turbidites existed to the east of the Fergana Basin up to the end of the Asselian. Since the beginning of the Artinskian, no marine deposits are known in the Tien Shan belt. We studied rocks of various lithologies from the West and Central Tien Shan (Fig. 1c).

Volcano-sedimentary rocks and lava flows were sampled from both limbs of a syncline in the Central Tien Shan (locality P). Flora remnants point to a Sakmarian–Artinskian age of these rocks (Masumov, 1994).

Red sandstones and conglomerates were studied from beds of various attitudes at localities RK (point R in Fig. 1c) and S. Redbeds unconformably overlay Asselian limestones and contain limestone debris with Sakmarian foraminifera. We also studied an entire section about 300 m thick of folded lacustrine sediments which conformably and with gradual transition overlie the redbeds (locality RA, point R in Fig. 1c). As the lacustrine sediments have a Kungurian–Ufimian flora, the underlying redbeds are of a late Early Permian age (Masumov, 1994).

Volcano-sedimentary rocks and lava flows were sampled from localities T and U in the northeastern part of the Chatkal Range. Both limbs of a syncline were studied at locality T, whereas bedding attitudes vary much less at locality U. These volcanics overlie sedimentary rocks with Asselian–Sakmarian foraminifera and Early Permian plants (Belgovsky, 1972; Masumov, 1994). Red sandstones with Kungurian–Ufimian flora (Masumov, 1994) disconformably overlying the volcanic series, were sampled at both localities; also sampled were lava boulders from conglomerates intercalating with the redbeds (locality T).

Terrigenous, sometimes tuffaceous, gray sandstones and siltstones with foraminifera of Asselian age (Masumov, 1994) were studied to the south of the Fergana Basin at localities V and W (Fig. 1c). Red conglomerates and sandstones disconformably overlying the Asselian gray rocks were sampled at locality W; these redbeds are of the Permian age, judging by flora remnants.

Everywhere, a hand-sample oriented with magnetic compass was sampled from a sedimentary layer or lava flow. Sampling points were spaced across the studied sections in such a way as to cover large stratigraphic intervals at each site. With a few exceptions, the true thicknesses studied at each site vary from several tens up to a few hundred meters.

3. Experimental procedures

One to three, usually two, cubic specimens from each hand sample were thermally demagnetized in 12–16 steps in home-made ovens with internal residual fields of about 10 nT. All measurements of natural remanent magnetization, NRM, were made on

a JR-4 spinner magnetometer with a noise level of 0.05 mA/m. The characteristic remanent magnetization (ChRM) was determined without anchoring the final linear segments to the origin of vector component diagrams (Kirschvink, 1980). ChRMs isolated from sister specimens of a hand sample were used to calculate sample means. As each sample mean represents an independent spot-reading of the paleofield, locality- and formation-means can be calculated at either the sample or site levels. Both are presented below in the tables; for interpretation, more conventional statistics at the site level were used.

4. Results

4.1. Volcanics of localities P and Q

Most samples of volcano-sedimentary rocks (Fig. 2a–b) and lava (Fig. 2c–d) responded well to thermal demagnetization, and a characteristic component, ChRM, shows the rectilinear decay to the origin, and this component was readily isolated above 350°C. ChRM directions are reversed and rather well clustered at each site except for in-situ data at site P6 where short-wave folds were sampled. Site-means are much better grouped after tilt-correction than in situ (Table 1; Fig. 2e–f), and the fold test (McElhinny, 1964) is positive at the 95% confidence level. The data grouping at 95% unfolding is better by just a few percent than that for fully unfolded data; the difference is certainly insignificant. At the same time, the calculated f statistics (McFadden and Jones, 1981) in stratigraphic coordinates slightly exceeds the critical value (Table 1). We account for this result by incomplete averaging-out of secular variations at each site and assume that a purely prefolding component was isolated at this locality.

The age of folding in this part of the Tien Shan is poorly constrained by a major unconformity between Permian and Paleogene rocks; all complexes are additionally deformed in the late Cenozoic. In other parts of this fold belt, however, Permian rocks are overlain with major unconformity by Jurassic and younger sediments, and most geologists believe that the folding took place in the Permian and, probably, partly in the Triassic. The isolated reversed ChRM precedes all deformation stages and, hence, is of Permian age.

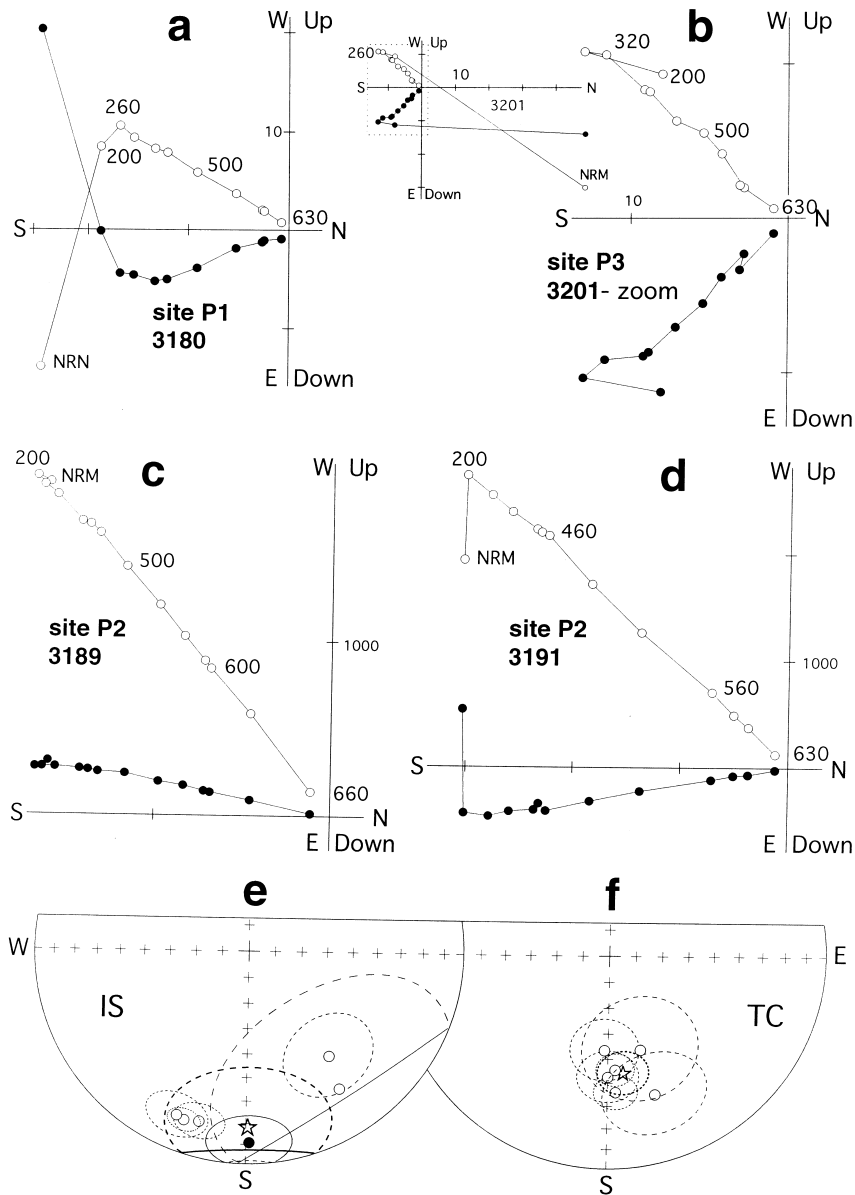


Fig. 2. Paleomagnetic results on volcano-sedimentary rocks from locality P. (a–d) Representative thermal demagnetization plots of volcano-sedimentary rocks (a,b) and volcanics (c,d) in stratigraphic coordinates. Dots (circles) represent vector endpoints projected onto the horizontal (vertical) plane. Steps are in degrees Celsius. Magnetization intensities are in mA/m. (e–f) Equal-area projection of ChRM site-mean directions together with their confidence circles (thin lines) and overall mean (star) with its confidence circle (thick dashed line) in situ (e) and after tilt correction (f). Open (solid) symbols and dashed (solid) lines are projected onto the upper (lower) hemisphere.

Paleomagnetic components isolated from volcanics at locality Q showed large scatter in both coordinate systems and during incremental unfolding, and the entire collection was discarded. This is

most probably due to heating, hydrothermal alteration and complex deformation during emplacement of a large granite intrusion nearby.

Table 1
Paleomagnetic results from locality P

Site	<i>N</i>	<i>Th</i>	<i>B</i>	In situ				Tilt-corrected			
				<i>D</i> (°)	<i>I</i> (°)	<i>k</i>	α_{95} (°)	<i>D</i> (°)	<i>I</i> (°)	<i>k</i>	α_{95} (°)
P1	7/6	50	250/39	195.2	−17.8	50	8.1	176.6	−36.0	59	7.4
P2	9/6	70	242/46	199.9	−16.2	122	5.2	176.3	−45.4	72	6.7
P3	6/6	30	250/44	202.6	−17.1	34	9.9	179.9	−42.5	29	10.7
P4	4/4	10	49/26	142.1	−38.0	18	16.4	161.2	−32.0	16	17.6
P5	5/4	12	174/64	179.0	10.9	31	12.6	182.1	−53.4	32	12.4
P6	3/3	5	119/33	146.1	−23.6	4	42.2	161.2	−51.6	15	21.0
Mean	29/34			185.6	−17.9	8	9.3	174.1	−43.0	26	5.1
	6			179.2	−18.6	8	25.8	172.6	−43.8	57	9.0
	$F_{(10,46)} = 2.04$			$f = 10.3$				$f = 2.14$			

N, number of samples (sites) studied/accepted; *Th*, true thickness studied in meters; *B*, mean azimuth of dip/dip angle; *D*, declination; *I* inclination; *k*, concentration parameter (Fisher, 1953); α_{95} , radius of cone of 95% confidence; $F_{(10,46)}$, 95% critical value of *F* statistics with the number of degrees of freedom in brackets; *f*, calculated values of the same statistics.

4.2. Sediments of localities RK, RA and S

Apart from an unstable dispersed component removed below 200° to 300°, the NRM in redbeds from localities RK and S is accounted for by two components. An intermediate-temperature component, ITC, persists over a large temperature range, from 200° until well above 600°C and accounts for the major part of NRM intensity. Sometimes, it decays to the origin (Fig. 3a,c); in most samples, however, the corresponding linear segments clearly miss the origin, and a high-temperature component, HTC, can be isolated (Fig. 3b,d). After tilt correction, the ITC points south to southeast and upward, whereas the HTC displays more easterly declinations and somewhat shallower inclinations. In a few samples with weaker reddish coloration or without it altogether (locality S), a single isolated component is directionally similar to that of the HTC in bi-component samples and was treated as such.

ITC site-mean directions from both localities are much better grouped after tilt correction than in situ (Tables 2 and 3; Fig. 4a–d). The fold test (McFadden and Jones, 1981) is positive for this component at locality RK (Table 2). At locality S, however, the 95% critical value is less than the calculated statistics; at the same time, the best data grouping is at 100% unfolding. We think that this pattern results from incomplete averaging of secular variations at some sites, and the ITC at locality S is of pre-folding origin too.

All modifications of the fold test are inconclusive for the HTC from locality RK due to the limited data set and small variation of bedding (Table 2; Fig. 4e–f). HTC site-mean directions from locality S are much better grouped after tilt correction than in situ (Table 3; Fig. 4g–h), and the same fold test is positive. The two tilt-corrected HTC locality-means agree very well (Tables 2 and 3; Fig. 5) and point to a pre-folding origin of this component everywhere. Judging by unblocking temperatures in redbeds and fold test results, the ITC is an overprint of pre-folding origin acquired during reddening and hematitization of redbeds, whereas the HTC is a primary component residing in detrital hematite (specularite).

An unstable scattered component of probably viscous origin in the lacustrine sediments from locality RA was easily removed after heating to 250° to 300°; after that, a ChRM showing a rectilinear decay to the origin was reliably isolated from most samples (Fig. 3e–f). Judging by NRM unblocking temperatures, the ChRM resides in magnetite in about a half of the collection, whereas hematite is the main NRM carrier in another. Magnetite and hematite samples alternate in the section, and the ChRM directions are the same irrespective of the remanence carriers (Table 2). This component is of reversed polarity, and the fold test (McFadden and Jones, 1981) is positive (Table 2; Fig. 4i–j).

There are, however, three samples from different sites where a component of normal polarity

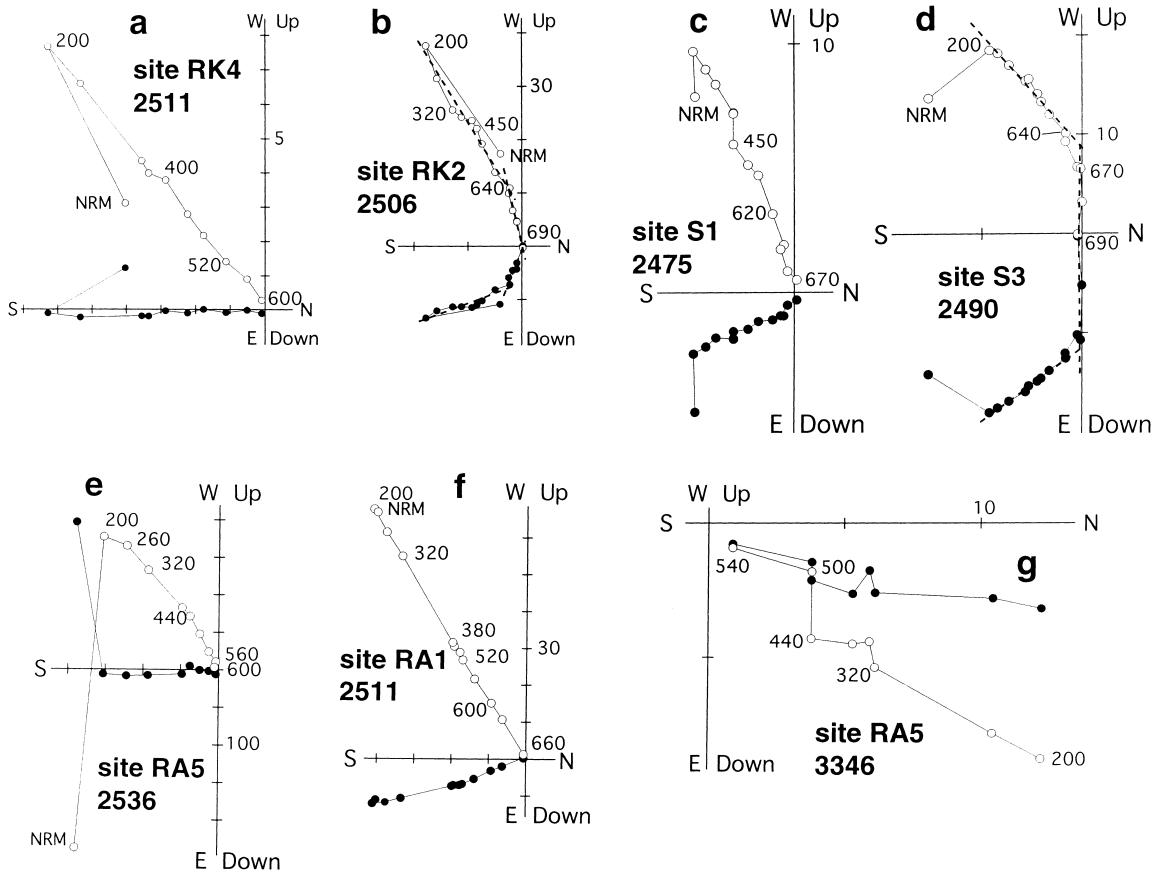


Fig. 3. Representative thermal demagnetization plots of redbeds from localities RK (a–b) and S (c–d) and lacustrine deposits from locality RA (e–g). Dashed lines denote isolated components (in bi-component samples only). Other notation as in Fig. 2a–d.

was identified despite noisier demagnetization data than for most samples with the reversed ChRM (Fig. 3g). These three normal directions are much better grouped in situ than after tilt correction, in sharp contrast to the reversed data (Table 2). It gives ground to the assumption that the normal polarity is a younger postfolding overprint and, hence, we exclude these three directions from computation of the formation-mean.

When all data from localities RK, RA and S are combined, a clear pattern appears (Fig. 5). The HTC in redbeds and the ChRM in younger lacustrine sediments are the end members greatly differing in declination and to a smaller but statistically significant degree, in inclination. The ITC directions fall in between but closer to the younger data. We see no other option but to account for such a pattern by a

rotation which occurred during the accumulation of the studied sequence. Hematization of redbeds had to take place closer to the end of this rotation and before accumulation of lacustrine beds which show uniform ChRM directions through the entire section.

The statistically significant difference in the ITC and HTC inclinations of $15.5^\circ \pm 7.4^\circ$ in redbeds from localities RK and S combined appears to imply a considerable time gap and northward motion between acquisition of these components. Against this, however, speaks the fact that the redbeds gradually change into lacustrine sediments without an erosional and/or angular unconformity. It is more likely to assume that there was no noticeable gap in accumulation of the entire studied section, but that the HTC inclination is shallowed which is quite probable for the detrital remanent magnetization residing

Table 2
Paleomagnetic results from locality RK and RA

Site	<i>N</i>	<i>B</i>	In situ				Tilt-corrected			
			<i>D</i> (°)	<i>I</i> (°)	<i>k</i>	α_{95} (°)	<i>D</i> (°)	<i>I</i> (°)	<i>k</i>	α_{95} (°)
Redbeds (RK)										
<i>Intermediate-temperature component</i>										
RK-1	5/5	237/10	165.7	−53.5	41	9.8	151.9	−55.5	46	9.3
RK-2	6/6	192/14	162.5	−44.8	18	13.3	152.5	−56.9	22	12.2
RK-3	5/4	204/25	178.7	−29.4	54	9.6	167.5	−51.3	131	6.1
RK-4	4/3	337/20	211.6	−73.5	366	4.2	180.7	−58.0	112	7.7
Mean	20/18		171.8	−49.4	15	8.6	160.5	−55.9	36	5.5
	4		174.4	−51.2	15	24.8	163.0	−56.0	99	9.3
	$F_{(6,28)} = 2.44$		$f = 7.6$				$f = 1.51$			
<i>High-temperature component</i>										
RK1	5/5	237/10	119.0	−50.4	18	14.9	110.4	−44.9	14	16.8
RK2+3 ^a	11/5	203/16	125.1	−38.4	10	20.3	111.4	−40.8	11	19.3
RK4	4/3	337/20	117.0	−50.5	86	8.7	126.8	−33.2	96	8.3
Mean	20/13		121.1	−46.0	16	9.6	115.1	−40.7	16	9.9
	3		120.7	−46.5	115	11.6	116.7	−39.9	76	14.3
	$F_{(4,20)} = 2.64$		$f = 0.56$				$f = 0.67$			
Lacustrine sediments (RA)										
RA1	8/7	283/17	213.6	−59.9	74	6.2	182.3	−61.4	63	6.7
RA2	6/6	280/15	200.4	−55.8	119	5.3	178.1	−55.6	117	5.3
RA3	4/4	177/30	169.5	−24.3	27	13.6	165.5	−54.1	23	14.5
RA4	5/4	180/30	184.1	−27.2	170	5.4	186.7	−57.3	139	5.9
RA5	5/4	343/30	220.9	−79.9	39	11.2	177.7	−54.1	33	12.2
RA6	5/5	351/24	227.4	−72.2	21	13.8	195.7	−53.3	26	12.2
RA7	3/3	316/42	290.7	−69.1	54	11.1	157.7	−65.6	49	11.6
Mean	39/33		200.2	−59.4	10	7.9	179.8	−57.7	40	3.9
	7		199.6	−60.1	8	22.5	178.4	−57.9	101	6.0
	$F_{(12,52)} = 1.94$		$f = 20.4$				$f = 1.76$			
NP	3		39.1	68.0	799	2.9	26.2	44.3	12	d23.2

^a Sites RK2 and RK3 combined.

NP: samples of normal polarity from different sites. Other notation as in Table 1.

in specularite. If so, both the rotation and hematitization of redbeds should be rather rapid. One may also speculate that the rotation triggered the latter process by increasing the permeability of the redbeds and at the same time forming a small basin where lacustrine sediments started accumulating.

4.3. Volcanics and redbeds localities T and U

Most volcanics and volcano-sedimentary rocks of these localities responded well to thermal demagnetization, and a well-defined ChRM was revealed (Fig. 6a,c–e); similar results were obtained by af

demagnetization on sister-specimens (Fig. 6b). The ChRM in most samples of volcanics is unblocked by 540° to 600° implying magnetite as the main carrier.

The dispersion of ChRM site-means decreases greatly after tilt correction, and the fold test (McElhinny, 1964) is positive at each locality (Table 4; Fig. 7a–d). The calculated *f* statistics (McFadden and Jones, 1981), however, are considerably larger than the 95% critical values (Table 4). The best data grouping is achieved at 100% unfolding at locality U, and a statistically insignificant maximum at 85% unfolding is observed at locality T. The structure of the latter locality is rather complicated, but it can

Table 3
Paleomagnetic results from locality S

Site	<i>N</i>	<i>Th</i>	<i>B</i>	In situ				Tilt-corrected			
				<i>D</i> (°)	<i>I</i> (°)	<i>k</i>	α_{95} (°)	<i>D</i> (°)	<i>I</i> (°)	<i>k</i>	α_{95} (°)
<i>Intermediate-temperature component</i>											
S1	6/8	110	10/40	58	−70	15	15.0	157	−61	41	9.0
S2	5/5	15	164/22	147	−27	46	9.3	140	−48	69	7.6
S3	8/8	70	164/36	159	−13	36	8.3	156	−50	43	7.6
S4	5/5	60	174/47	163	−6	105	6.1	155	−53	88	6.7
S5	5/8	80	172/72	150	24	53	8.6	143	−42	46	9.2
Mean	29/34			150	−20	4	12.5	150	−51	39	4.2
	5			150	−20	4	45.3	150	−51	88	8.2
	$F_{(8,48)} = 2.14$			$f = 41.6$				$f = 3.17$			
<i>High-temperature component</i>											
S1	8/8	110	11/38	89	−42	14	13.4	124	−37	24	10.1
S2–4	7/18	155	171/42	135	−7	13	14.6	121	−40	19	12.3
S5	5/8	180	177/75	122	8	48	9.1	107	−30	53	8.6
Mean	20/34			117	−18	6	13.0	119	−36	23	6.5
	3			118	−14	6	55.4	117	−36	80	13.9
	$F_{(4,34)} = 2.64$			$f = 16.7$				$f = 1.69$			

^a Sites S2, S3 and S4 combined. Same notation as in Table 1.

hardly account for misfit of ChRM directions as the sites from different limbs differ both in declination and inclination (e.g., sites T1–3 and T4–5, Table 4).

When the results from both localities are pooled, the fold test (McElhinny, 1964) points to a pre-folding age of the ChRM (Table 4, Fig. 7e). The other test, however, gives a significant value of *f* statistics (McFadden and Jones, 1981), and a statistically insignificant maximum at 85% unfolding is present. As each site is based on a small number of samples, and secular variation is perhaps inadequately averaged out, we pooled the sites with similar attitudes (T1–T3 and T4–T5, U1–U3 and U4–U5) and re-applied the fold test (McFadden and Jones, 1981) which again yielded large values of *f* statistics. Primary tilts are quite plausible in these subaerial volcanics, in particular for locality T where the rocks accumulated in a graben-like structure, thus accounting for ‘imperfectness’ of the fold test. This source of paleomagnetic noise would be better averaged out if sampling sites are spread over a larger area; hence, all data were pooled, and an overall mean for two localities was computed (Table 4).

A single ChRM was reliably isolated from redbeds (Fig. 6f–g) which overlie the volcanics at

both localities. The fold test is inconclusive for each locality separately due to almost uniform bedding attitudes and definitely positive for the combined redbed data (Table 4, Fig. 7f–g).

Debris and rounded boulders of lava visibly similar to, but somewhat more altered than, underlying volcanics were sampled from conglomerates intercalated with redbeds at locality T. Some samples revealed a single component (Fig. 6h), whereas others showed two distinct components (Fig. 6i). The component isolated below 570°–600° is scattered (Fig. 7h), and the normalized vector-resultant of 0.24 is much less than the critical value of 0.44 (Mardia, 1972); hence, the conglomerate test is positive. In contrast, the high-temperature component, HTC, is rather well grouped, and its mean direction is indistinguishable from the ChRM in redbeds (Table 4; Fig. 7g). The similarity of the HTC in conglomerates and the ChRM in redbeds implies that acquisition of the latter affected lava debris during hematitization of these sedimentary rocks. There are, however, no signs of a hematite component with similar direction in underlying volcanics (Fig. 6a–e), and it is unlikely that the scatter of data on volcanics results from a partial overprinting by the ‘redbed’ component.

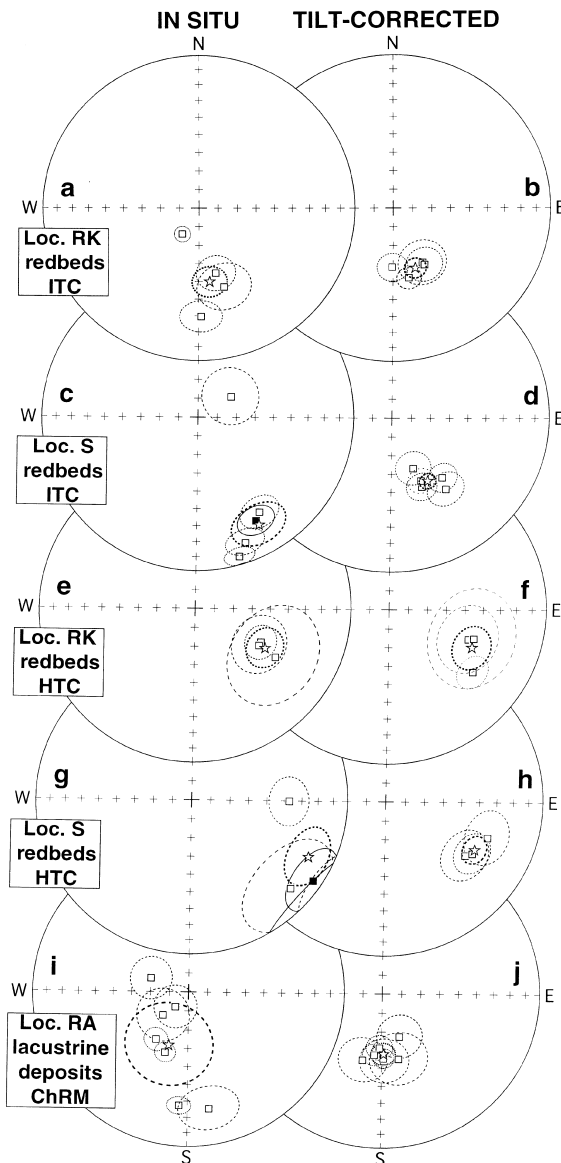


Fig. 4. Equal-area projection of site-means (squares) with associated confidence circles (thin lines) and locality-mean directions (stars) with confidence circles (thick lines) from localities RK (a–b, e–f), RA (i–j) and S (c–d, g–h). *ITC* (a–d) and *HTC* (e–h) are intermediate- and high-temperature components in redbeds, respectively. *ChRM* is the characteristic component in lacustrine deposits from locality RA (i–j). Other notation as in Fig. 2e–f.

4.4. Volcano-sedimentary rocks of locality V

Thermal demagnetization revealed a well-defined component, isolated above 200° to 300° from most

samples of this locality. This intermediate-temperature component persists up to 540° to 580°, implying magnetite as its carrier and usually misses the origin (Fig. 8a). Also, many samples display remagnetization circles over a wide temperature range. This indicates the presence of another component, *HTC*, which, however, could be properly isolated from only three samples from site V6 (Fig. 8b). This failure is partly due to strong mineralogical alteration in many samples above 450°–500° (Fig. 8c) which prevented further treatment.

ITC site-means are scattered both in situ and after tilt correction (Table 5, Fig. 8d–e). A closer inspection shows that the mean vector of site V2 deviates from other data at all steps of unfolding; after its omission, the other site-means define a distinct and statistically significant maximum at 60% step of unfolding (Fig. 8f–g) implying a synfolding origin of the *ITC*.

A similar pattern may appear if the *ITC* and *HTC* in these rocks have strongly overlapping unblocking spectra which is difficult to recognize from a true synfolding component. In this case, however, the normals to remagnetization circles are scattered both in situ and after tilt correction (Fig. 9a–b), whereas they display a much better grouping at 50% unfolding (Fig. 9c). This finding is difficult to explain by overlapping unblocking spectra; in contrast, it is just what should be expected if the least-dispersed component, the *ITC* in this case, is of a synfolding origin.

4.5. Volcano-sedimentary rocks and redbeds of locality W

After removal of an unstable component above 200° to 300°C, an intermediate-temperature component, *ITC*, was isolated from most samples (Fig. 10). This component persists to 500° to 600°, and is likely to be carried by magnetite. The corresponding linear segments usually do not pass through the origin; a *HTC*, however, could be isolated only from redbed samples and a few samples of grayish rocks (Fig. 10d,e); in the latter, a better *HTC* isolation was prevented by acquisition of spurious components above 500°C.

ITC site-mean directions from this locality are much better grouped after tilt correction than in situ

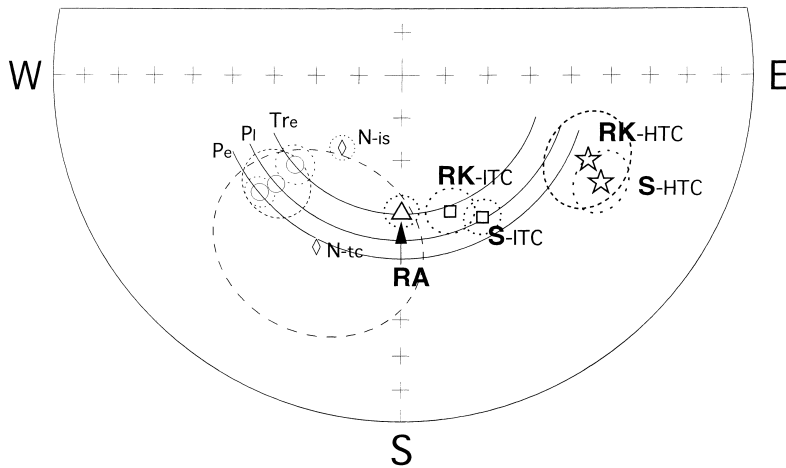


Fig. 5. Equal-area projection of locality-mean directions of isolated components from localities S, RK and RA and Eurasian reference directions Van der Voo, 1993 with their confidence circles. Squares and stars: ITC and HTC directions from redbeds, respectively. Triangle: ChRM direction from lacustrine deposits from locality RA. Diamonds: in-situ (*is*) and tilt-corrected (*tc*) mean directions for samples of normal polarity in lacustrine deposits from locality RA. Circles: European reference directions. Thin solid lines are reference inclinations drawn to facilitate comparison. All data except for N-*is*, are in stratigraphic coordinates. All symbols are projected onto the upper hemisphere.

Table 4
Paleomagnetic results from localities T and U

Site	<i>N</i>	<i>Th</i>	<i>B</i>	In situ				Tilt-corrected			
				<i>D</i> (°)	<i>I</i> (°)	<i>k</i>	α_{95} (°)	<i>D</i> (°)	<i>I</i> (°)	<i>k</i>	α_{95} (°)
T1-V	5/4	150	188/32	157.2	-29.5	52	9.7	138.2	-54.6	152	5.7
T2-V	6/6	200	160/53	148.1	-11.0	44	8.6	136.0	-61.3	24	11.6
T3-V	7/4	250	151/35	149.3	-26.1	67	8.5	147.1	-61.4	86	7.6
T4-V	6/5	120	48/36	105.1	-30.9	78	7.1	123.0	-41.8	82	6.9
T5-V	5/3	30	7/54	78.2	-33.1	41	12.7	117.4	-32.8	79	9.1
Mean	29/22			132.7	-27.4	8	10.4	130.8	-52.2	25	6.0
	5			129.7	-29.5	7	31.2	130.0	-50.9	30	14.1
T6-RB	4/4	30	254/13	188.3	-50.9	41	10.9	171.6	-54.6	97	7.1
T7-RB	4/4	30	203/16	178.4	-44.9	134	6.1	167.5	-59.1	118	6.5
T8-C ^a	16/9		224/13	187	-43	20	10.6	179	-58	20	10.5
U1-V	6/4	120	133/50	139.7	-9.3	62	8.9	145.8	-58.8	61	9.0
U2-V	6/4	50	134/51	134.7	-19.1	86	7.6	135.4	-68.1	69	8.4
U3-V	7/4	150	133/50	118.4	-20.0	17	16.9	96.6	-66.4	17	16.9
U4-V	5/4	130	147/94	119.3	31.1	50	9.9	108.3	-52.5	71	8.3
U5-V	5/4	150	143/79	127.5	14.7	160	5.6	113.8	-59.5	40	11.2
Mean	27/20			128.2	-0.6	11	9.5	119.8	-62.2	28	6.0
	5			128.2	-0.7	11	23.8	119.7	-62.2	51	10.8
U6-RB	6/6	15	199/90	181.4	29.2	45	8.6	170.5	-55.2	51	8.0
All V	10			128.9	-14.8	7	19.0	125.6	-56.7	33	8.5
	$F_{(18,64)} = 1.77$			$f = 24.0$				$f = 4.99$			
All RB	3			182.4	-24.2	4	80.3	170.0	-56.3	898	4.1
	$F_{(4,22)} = 2.81$			$f = 70.4$				$f = 0.33$			

^a Secondary component from conglomerate.

V, RB and C after site numbers stand for volcanics, redbeds and conglomerates, respectively. Other notation as in Table 1.

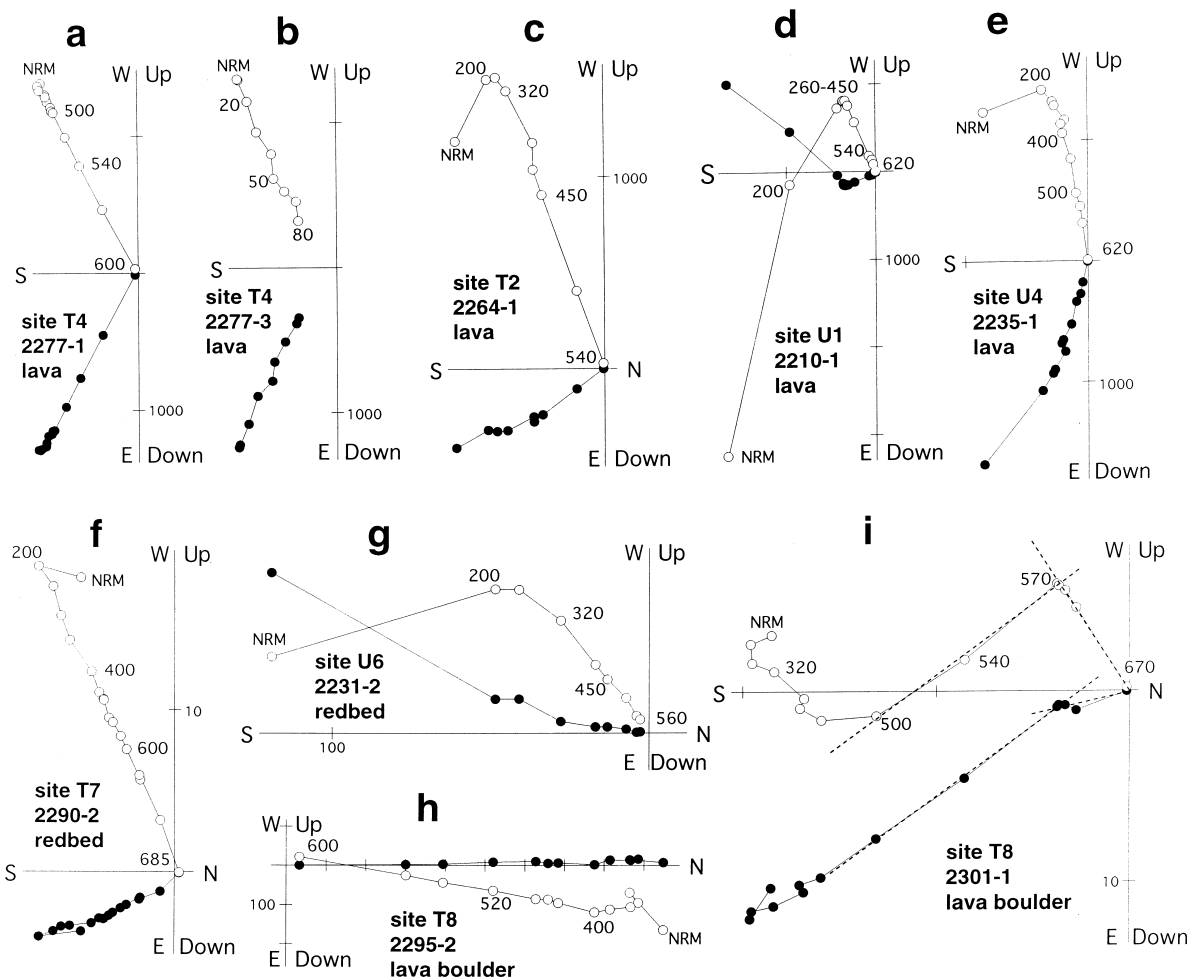


Fig. 6. Representative thermal (a, c–i) and AF (b) demagnetization plots of lava (a–e) and redbed (f–g) samples and lava boulders from conglomerates (h–i) from localities T and U. Same notation as in Fig. 2a–d.

(Table 6; Fig. 11a,b). Despite the best grouping of site-means at 100% unfolding, the fold test (McFadden and Jones, 1981) yields a significant value of f statistics (Table 6) which we failed to unambiguously account for. Tentatively, we regard the ITC as a prefolding overprint. In contrast, the same test indicates that the HTC in these rocks is prefolding and most probably primary (Table 6; Fig. 11c,d).

4.6. Summary of paleomagnetic results

Except for three samples from locality RA where a postfolding remagnetization is suspected, all isolated intermediate- and high-temperature compo-

nents are of reversed polarity. This finding agrees with remanence acquisition during the Kiaman reversed superchron, i.e., before 250 Ma, in all rocks. Since the studied rocks are of an Early to early Late Permian age, the ages of isolated components, including the overprints and synfolding components, are close to the rock ages.

At the same time, two directionally distinct groups of paleomagnetic directions can be recognized in the West Tien Shan. One group incorporating the primary directions from the youngest formations (localities RA, T, and U) and overprints in the older formations (localities RK, S, and W), has southerly to southeasterly declinations. The other

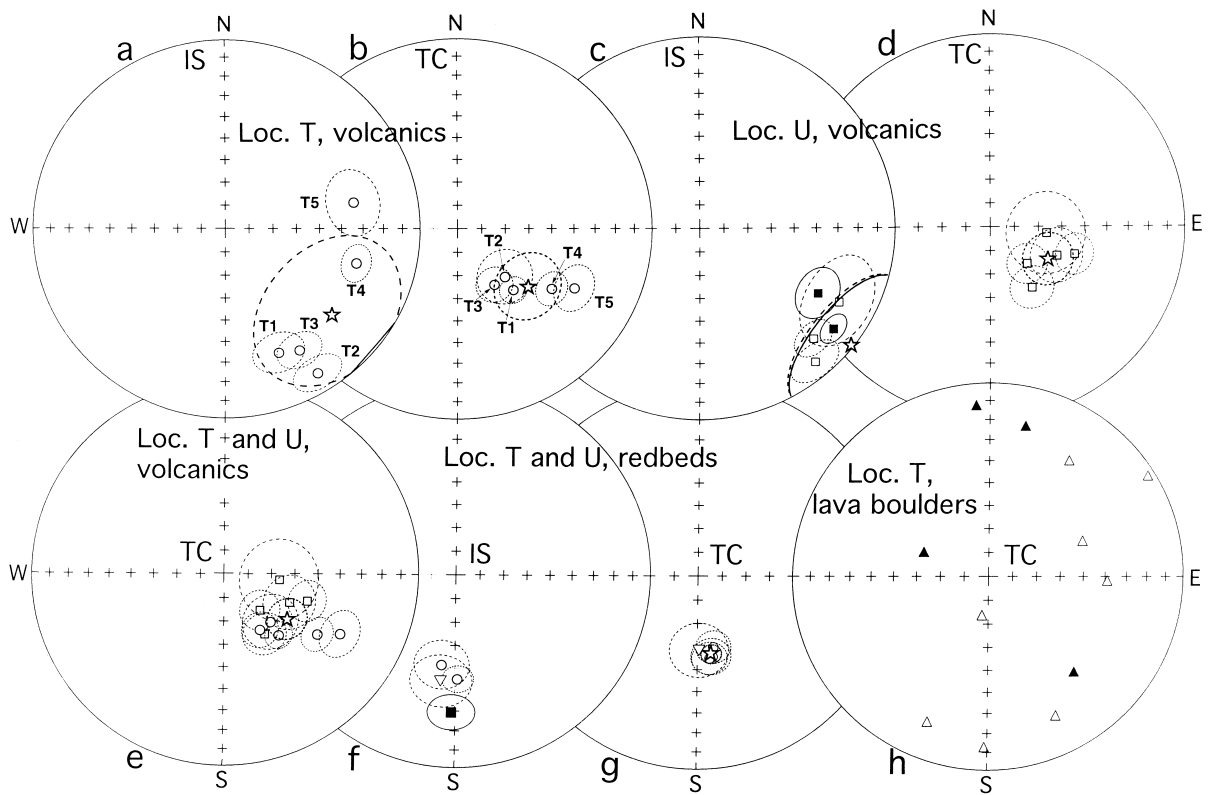


Fig. 7. Equal-area projection of paleomagnetic directions on volcanics (a–e), redbeds (f–g) and conglomerates (h) from localities T and U. Circles and squares are site-means with associated confidence circles (thin lines) from localities T and U, respectively. Stars and thick lines are locality-mean (a–d) and overall mean (e–g) directions with associated confidence circles (thick lines). Inverted triangle (in f, g) is the mean hematite component in conglomerates (see text for explanation) shown for comparison and not included into overall mean on redbeds. IS and TC are for in-situ and tilt-corrected data, respectively. Triangles: directions of magnetite component in lava boulders from conglomerate (loc. T). Other notation as in Fig. 2e,f.

Table 5
Paleomagnetic results locality V

Site	N	B	In situ				Tilt-corrected			
			D (°)	I (°)	k	α_{95} (°)	D (°)	I (°)	k	α_{95} (°)
V1	5/4	9/74	76.2	-63.8	10	22.2	162.6	-24.3	12	20.4
V2 ^a	7/5	353/104	70.5	-39.6	58	8.2	125.0	-1.1	37	10.3
V3	4/4	18/56	85.2	-54.9	164	5.5	153.9	-37.9	160	5.5
V4	7/6	164/20	137.2	-38.8	82	6.3	124.0	-56.7	49	8.2
V5	10/9	174/38	158.6	-35.9	38	7.6	135.1	-70.3	38	7.6
V6	5/5	173/37	159.0	-29.4	35	10.6	145.4	-62.9	37	10.4
V7	4/4	142/20	149.2	-47.7	92	7.3	153.7	-67.0	46	10.4
Mean	42/32	141.5	-46.0	10	7.8	145.3	-57.5	14	6.5	
U60	6		135.9	-49.4	10	22.7	148.5	-54.1	16	17.0
U60	6		146.2	-54.3	124	6.1				

^a Rejected site (see text for explanations).

U60, mean direction after 60% unfolding. Other notation as in Table 1.

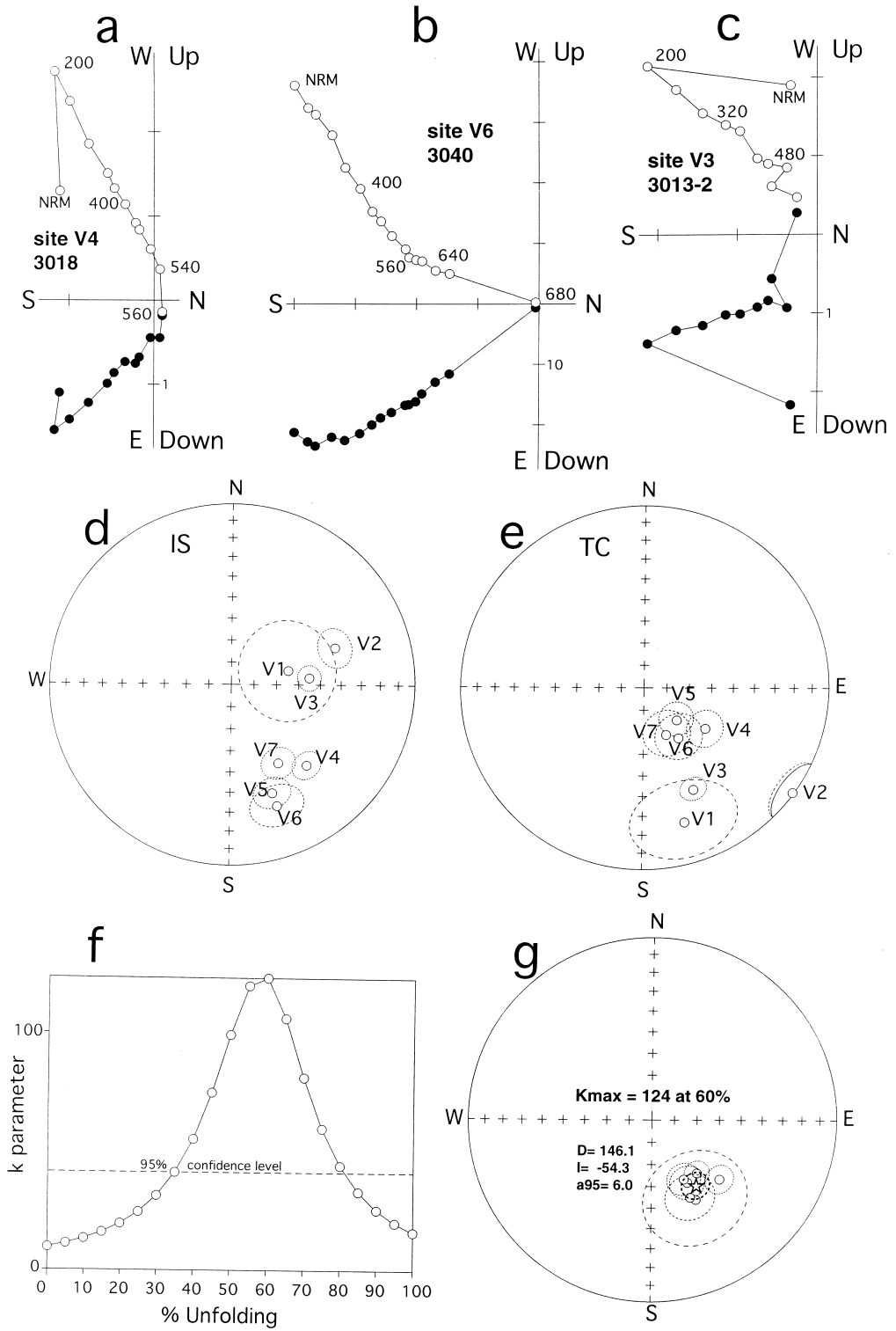


Table 6
Paleomagnetic results from locality W

Site	<i>N</i>	<i>Th</i>	<i>B</i>	In situ				Tilt-corrected			
				<i>D</i> (°)	<i>I</i> (°)	<i>k</i>	α_{95} (°)	<i>D</i> (°)	<i>I</i> (°)	<i>k</i>	α_{95} (°)
<i>Intermediate-temperature component</i>											
W1	11/7	120	186/68	163.9	11.2	26	10.4	151.4	−48.6	33	9.2
W2	8/6	100	169/57	158.6	13.0	86	6.2	154.9	−42.2	101	5.7
W3	10/7	80	21/18	118.1	−40.2	36	8.9	130.9	−36.0	44	8.0
W4	10/10	60	132/19	132.8	−24.9	60	5.7	139.2	−43.6	72	5.2
Mean	39/30			143.3	−13.1	7	9.5	142.8	−43.1	37	4.2
	4			145.2	−10.6	6	40.8	142.1	−43.1	60	12.0
	$F_{(6,52)} = 2.28$			$f = 45.8$				$f = 5.13$			
<i>High-temperature component</i>											
W1+2	19/4	220		138.1	1.4	16	17.7	122.7	−41.3	20	15.7
W3	10/8	80	21/18	92.2	−31.0	21	10.8	103.4	−34.9	31	8.9
W4	10/8	60	113/21	114.9	−23.1	38	8.1	116.4	−44.0	32	8.7
Mean	39/20			111.4	−22.4	10	9.8	112.0	−40.1	25	6.2
	3			116.3	−18.7	9	44.2	113.7	−41.0	80	13.9
	$F_{(4,34)} = 2.64$			$f = 13.3$				$f = 2.22$			

Same notation as in Table 1.

group including the HTC data on older rocks, has more easterly declinations. A similar pattern was also found in the southwestern part of the Tien Shan (Fig. 1c, loc. A and B) (Bazhenov et al., 1993). Judging by the rock ages from locality R where this transition is best constrained, the boundary between these two directional groups is of Artinskian–Kungurian age (ca. 250–260 Ma).

5. Analysis of inclinations from the Tien Shan and adjacent regions

The Tien Shan is far away from the European, Siberian and Indian cratons and, in principle, its affinity with either plate in the Permian should be tested using corresponding apparent polar wander paths (APWP). The Indian APWP (Van der Voo, 1993) predicts high southern latitudes for the Tien Shan, in drastic contrast to the observed middle northern latitudes. It is not clear a priori whether

Siberia and Europe had already welded together by that time as crustal shortening in the Urals and Kazakhstan spanned the entire Permian; hence, a comparison should be made for each of these two continents separately. Unfortunately, the Permian (without further subdivision) Siberian mean pole is based on rather scattered data (Khramov et al., 1982) which are in turn based on poorly cleaned collections. In addition, many Late Permian Siberian poles are from the Siberian traps and are very close to the Permo–Triassic boundary and thus younger than most data from the Tien Shan.

Better defined Early and Late Permian European poles (Van der Voo, 1993) were used to calculate paleomagnetic directions, and these were compared with Permian results from the Tien Shan, Tarim, Pamirs and Kazakhstan. The values of flattening $F = I_r - I_m$, where I_r and I_m are the reference and measured inclinations, respectively, and the error limits ΔF were calculated after Demarest (1983); a positive (negative) F value implies a northward

Fig. 8. Paleomagnetic results on volcano-sedimentary rocks from locality V. (a–c) Representative thermal demagnetization plots. Same notation as in Fig. 2a–d. (d–e, g) Equal-area projection of ChRM site-mean directions (circles) together with their confidence circles in situ (d), after tilt correction (e) and after 60% unfolding (g). Other notation as in Fig. 2e,f. (f) Plot of concentration parameter (*k*) versus percent of unfolding for six site-means. In (f) and (g), site V2 is omitted.

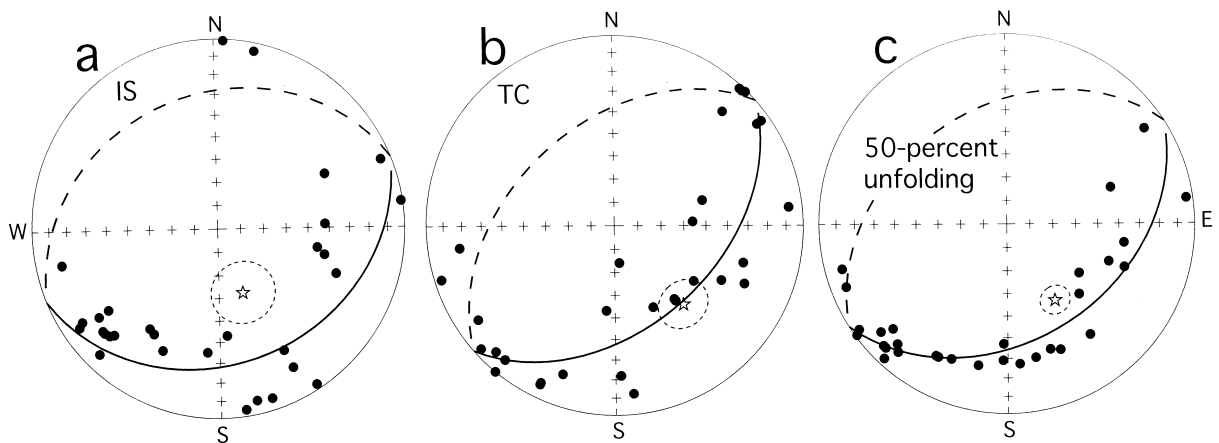


Fig. 9. Equal-area projection of normals to remagnetization circles (dots) and direction of the least-dispersed component (star) with confidence circle for volcano-sedimentary rocks from locality V in situ (a), after tilt correction (b) and after 60% unfolding (c). Other notation as in Fig. 2e,f.

(southward) motion of the study area. We included in the analysis all Permian data based on complete stepwise demagnetization and component analysis (Table 7) and discarded the results from the West and Central Tien Shan which were obtained with the aid of blanket cleaning at low to moderate temperatures and alternating fields. This omission is justified by rather complicated demagnetization patterns revealed by our study.

The plots of F values versus present-day longitude were made separately for the Early and Late Permian data (Fig. 12). The Early Permian set includes primary components isolated from Lower Permian rocks, whereas the second set comprises both primary components from the Upper Permian rocks and secondary components from the older formations. Since the Tien Shan stretches almost due E–W, such plots give a fairly good reflection of inclination variation along the fold belt. It is immediately clear that there is no systematic change of F values along the Tien Shan. It is also clear that most results from the Tien Shan belt and adjacent areas are statistically indistinguishable from the European reference data, with several exceptions which deserve a more detailed inspection (Table 7, Fig. 12). If the Early Permian pole is used, the volcanics from the Chatkal Range (localities T and U) yield the statistically significant lowest F value of $-11 \pm 7^\circ$ (Fig. 12a). As discussed above, these subaerial volcanics might have accumulated on uneven surfaces where some

primary tilts are possible. So it might be that even the combined collection from both localities is not sufficient to adequately average out these errors. On the other hand, these volcanics might well have a late Early Permian age. As the time window used for calculation of the mean Late Permian pole encompasses a part of the Early Permian, the Chatkal result was also compared with this reference pole; such a procedure leads to an F value of $7 \pm 8^\circ$ which is marginally insignificant (Table 7, Fig. 12b).

Two significant F values, one positive and one negative, are from a small part of North-West Tarim where three studies on Permian rocks yielded very different inclinations (entries M–O, Table 7). Clearly something is wrong in the paleomagnetic kingdom. Some rather large positive F values involve sedimentary rocks where the inclination error is suspected (D, RK1, S1). Finally, the H result is a secondary component in older rocks (Zhao et al., 1990) where the paleohorizontal is not as accurately determined as for primary components in stratified formations.

Paleomagnetic poles certainly did not move by jumps, but one has to use rather wide time windows to construct an APWP. So, the use of a mean pole as a reference will lead to errors if the ages of studied rocks and/or remanences are close to the time window margins; unfortunately, an APWP with a better time resolution is not available. Both rock ages and the ages assigned to paleomagnetic components are also imprecise as follows from the above text, and

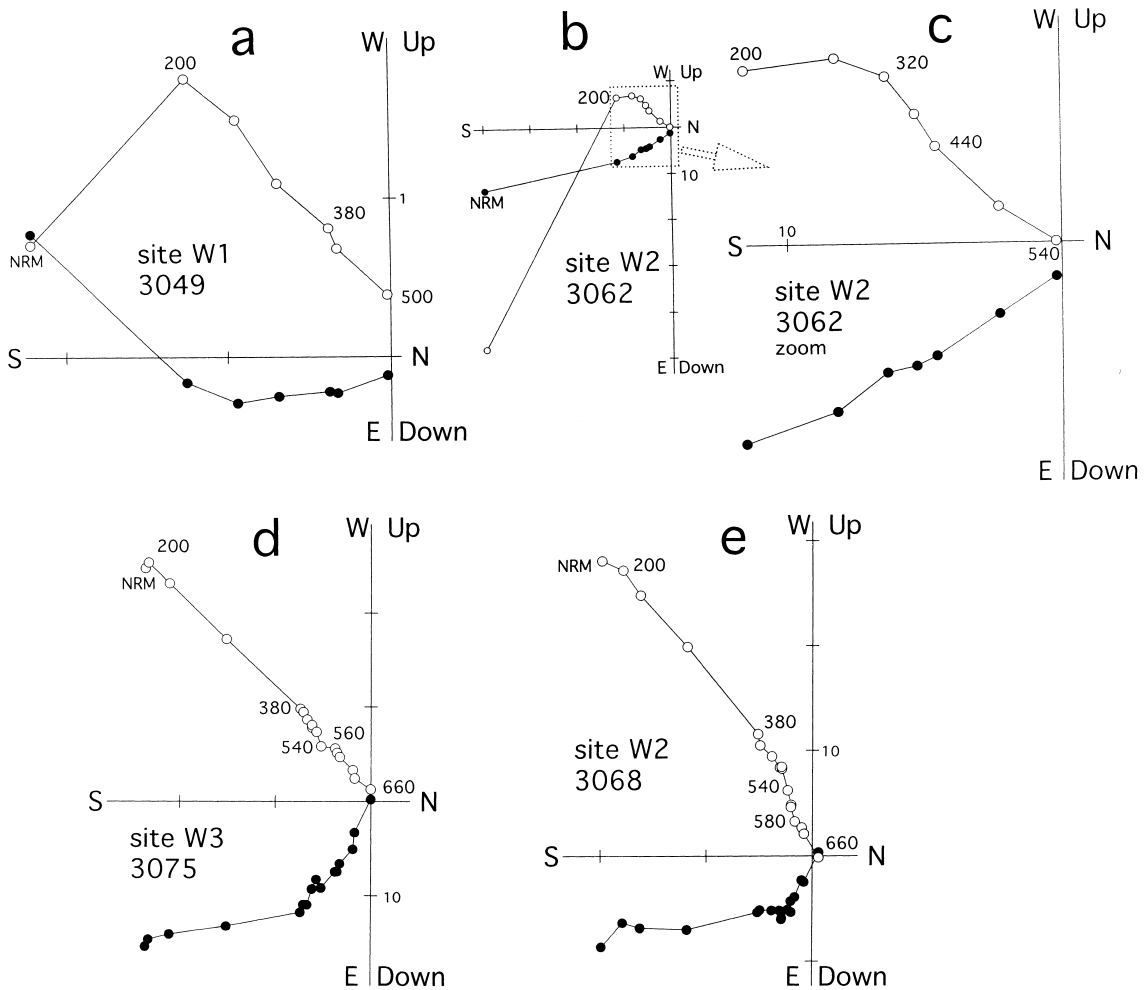


Fig. 10. Representative thermal demagnetization plots of volcano-sedimentary rocks (a–c) and redbeds (d–e) from locality W. Same notation as in Fig. 2a–d.

these age-related errors certainly contribute to the observed scatter.

Except for the above-discussed negative values (M, T + U), the other Early Permian results yield positive F values. Without these two anomalies, the overall mean of this parameter is 4.4° . Unfortunately, it is impossible to calculate the confidence limits for this result. In the Late Permian data set, the results, though scattered, show no systematic shift with respect to the abscissa. Taken at face value, a very moderate convergence may be hypothesized between the Tien Shan and Europe in the Early Permian. However, a possible influence of inclination error

suspected in some results (RK1, S1) may further diminish the magnitude of convergence. Our analysis also shows that, since the Late Permian, the shortening of the Tien Shan, including that due to the India–Eurasia collision, is within the uncertainties of the available data

Permian data from Kazakhstan (KZ) and South Tarim (ST) are also included in the analysis (Table 7). The Permian result from Kazakhstan which is three decades old (Kumpan et al., 1968) and does not satisfy modern standards, nevertheless agrees quite well with the reference data. New Permian results from South Tarim (Gilder et al., 1996) are also in accord

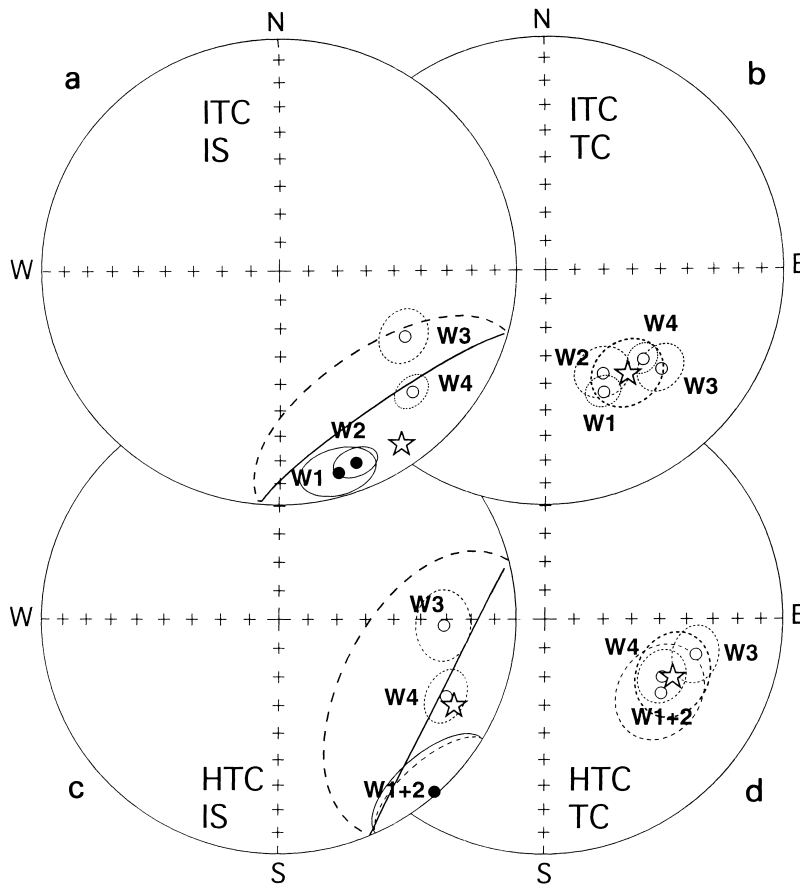


Fig. 11. Equal-area projection of site-means (circles) of the ITC (a–b) and HTC (c–d) with associated confidence circles (thin lines) and locality-mean directions (stars) with confidence circles (thick lines) from locality W in situ (a, c) and after tilt correction (b, d). Other notation as in Fig. 2e,f.

with the reference data (Table 7). This finding implies that the relative latitudinal displacements between the East European platform, Kazakhstan, Tien Shan and Tarim lie within the uncertainties of available data at least since the mid-Permian. This is in contrast to the assumption of Gilder et al. (1996) that Tarim could be separated from Eurasia in the Permian. The disagreement most probably stems from the choice of the Siberian APWP which is more poorly defined than the European one used in this work.

6. Declination pattern and kinematics of rotation

The new results reveal northerly to northwesterly to sometimes almost westerly declinations when

inverted to normal polarity. There is also a clear tendency for the older components to deflect more westward in comparison to the results on younger rocks and/or the overprints to the west of the Talas–Fergana Fault, in accord with the results from the South-West Tien Shan (A and B, Bazhenov et al., 1993). In general, the data to the east of this fault irrespective of their age indicate smaller rotations (Table 7, Fig. 13).

When compared with the European Permian reference poles (Van der Voo, 1993), all observed declinations from the Tien Shan fold belt sensu stricto and adjacent parts of Tarim and Junggar are systematically CCW rotated through varying angles (Table 7). Such a consistency of the sense, if not the angle, of rotation favors a common source for the declination pattern.

Table 7

Observed and reference paleomagnetic directions and kinematic parameters of the Tien Shan and adjacent areas

L	COM	AGE	I_m (°)	I_r (°)	$F \pm \Delta F$ (°)	D_m (°)	D_r (°)	Ro (°)	Ro1 (°)	REF
A	PR	Pe	39	42	3 ± 4	325	51	86 ± 5	39 ± 7^e	1
B	PR	Pl	48	47	-1 ± 5^a	8	48	41 ± 6		1
C	PR	Pe	41	44	3 ± 2	327	52	85 ± 4		2
D	OV	Pl	42	51	9 ± 4	36	52	16 ± 4		3
E	PR	P	46	51	5 ± 3	55	56	1 ± 4		4
F	PR	P	48	51	3 ± 5	343	56	73 ± 8		4
G	PR	P	49	50	1 ± 3	33	55	22 ± 5		4
H	PR	Pe	50	57	7 ± 4	48	61	13 ± 7		5
I	PR	Pl	62	61	-1 ± 4	343	57	74 ± 8		6
J	PR	Pl	59	62	3 ± 7	7	58	51 ± 10		7
K ^a	PR	P–Te	55	58	3 ± 5	22	55	33 ± 9		8
L	PR	Pl	50	54	4 ± 4	28	52	24 ± 7		9
M	PR	Pe	58	51	-7 ± 3	32	56	24 ± 5		10
N	PR	Pe	50	51	1 ± 3	42	56	14 ± 5		11
O	PR	Pe	41	51	10 ± 4	34	56	22 ± 6		11
P	PR	P	44	48	4 ± 7	353	54	61 ± 10		TP
RA	PR	Pl	58	52	-6 ± 6	358	51	53 ± 11		TP
RK ₂	OV	Pl	56	52	-4 ± 8	343	51	68 ± 15		TP
RK ₁	PR	Pe	40	47	7 ± 12	297	54	117 ± 15	64 ± 18	TP
S ₂	OV	Pl	51	52	1 ± 10	330	52	82 ± 12		TP
S ₁	PR	Pe	36	47	11 ± 11	297	54	117 ± 14	35 ± 18	TP
T+U	PR	Pl	56	50	-6 ± 5	350	50	60 ± 8		TP
T+U	PR	Pe	57	46	-11 ± 7	306	53	107 ± 13	44 ± 14	TP
T+U ^b	PR	Pl	57	50	-7 ± 8	306	50	104 ± 14		TP
V ^c	SYN	Pl?	54	49	-5 ± 6	326	49	83 ± 10		TP
W ₂	OV	Pl	43	49	6 ± 10	322	49	87 ± 14		TP
W ₁	PR	Pe	41	44	3 ± 11	294	52	118 ± 15	31 ± 20	TP
TR	PR	Tm–l	70	63	7 ± 6	355	55	60 ± 16		1
ST ^d	PR	P	52	51	1 ± 7	30	52	22 ± 11		12

^a The average of Late Permian and Early Triassic reference values was used.^b Early Late Permian age of this result is assumed (see text for discussion).^c A Late Permian age is assigned.^d The average of Early and Late Permian reference values was used following Gilder et al. (1996).^e Angular difference between Early Permian result from loc. A and Late Permian result from loc. B.

L is locality labeled as in Fig. 1c and Fig. 13 continuing the notation of Bazhenov et al. (1993). Indices 1 and 2 are for primary and secondary NRM components, respectively. Permian result from South Tarim (ST) and Triassic result from the West Tien Shan (TR) (not shown in the figures) are added. COM = paleomagnetic component: PR, primary; OV, secondary pre-folding; SYN, synfolding. AGE = age of paleomagnetic component: P, Permian; T, Triassic; e, Early; m, Middle; l, Late. D and I are declination and inclination (inverted to normal polarity); subscripts m and r denote measured and reference data, respectively. F is flattening with interval of confidence (ΔF); Ro is rotation angle of the observed declination with respect to the coeval reference value; Ro1 is the difference between Early and Late Permian declinations for the West Tien Shan results; positive values stand for counterclockwise rotation. The confidence limits were computed as suggested in Demarest, 1983. References: TP, this paper; 1, Bazhenov et al., 1993; 2, Bazhenov et al., 1995; 3, Bolshakov et al., 1989; 4, Audibert and Bazhenov, 1992; 5, Zhao et al., 1990; 6, Sharps et al., 1992; 7, Nie et al., 1993; 8, McFadden et al., 1988; 9, Li et al., 1988a; 10, Sharps et al., 1989; 11, Bai et al., 1987; 12, Gilder et al., 1996.

For the West Tien Shan, where a two-phase rotation is found, the older movements most probably took place close to the Early–Late Permian boundary (Kungurian–Ufimian) as inferred by the ages of the studied rocks. The age of younger rotation in the

same area is not clear, but it certainly postdates the age of the youngest formations (Kungurian–Ufimian, localities R–U). The Late Permian data from the Urumque area (I, J) (Sharps et al., 1992; Nie et al., 1993) and Late Permian–Early Triassic result from

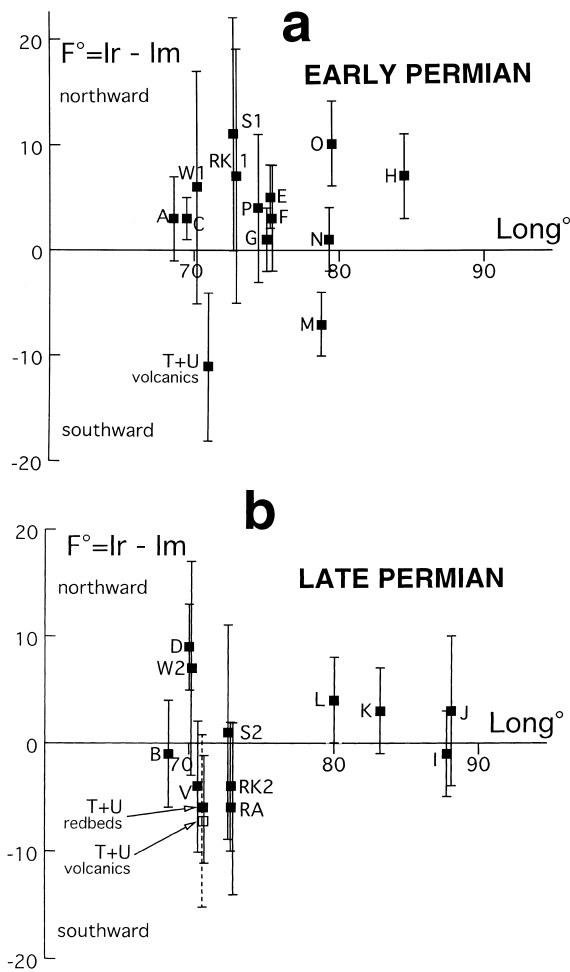


Fig. 12. Plots of parameter F ($= I^{\circ}_{\text{reference}} - I^{\circ}_{\text{measured}}$) versus present-day longitude for the Early (a) and Late (b) Permian data. Each result (square) is shown with associated error bars calculated at the site-mean level. Combined result on volcanics from localities T and U on the Late Permian plot (b) (open square and dashed error bar) is shown to illustrate age-related errors (see text for details). RK2 (RK1), S2 (S1) and W2 (W1); secondary (primary) components at localities RK, S and W. Other localities are labeled as in Fig. 1, Table 7 and the text.

the Aksu area (K) (McFadden et al., 1988) in China are also rotated (Table 7, Fig. 13).

Paleomagnetic results on Lower Cretaceous and Paleogene rocks point to about 20° CCW rotations of an area to the southwest of the Talas–Fergana Fault (Bazhenov, 1993; Thomas et al., 1993; Bazhenov et al., 1994a). As these rotations are much smaller than those indicated by the Permian results, the

latter were not corrected for younger rotations. In the southwestern Tien Shan, however, no detectable Cenozoic rotations were found (Bazhenov et al., 1994b). Neither Paleogene nor Cretaceous paleomagnetic data show discernible Cenozoic rotations to the east of the Talas–Fergana Fault up to the Turfan Basin (Li et al., 1988b; Chen et al., 1991, 1992; Thomas et al., 1993; Cogné et al., 1995). Jurassic coal-bearing rocks from several localities over the Tien Shan were shown to bear only a present-day postfold component (M.L. Bazhenov, unpublished data; A.F. Eroshkin, pers. commun.). The only result on Middle–Upper Triassic lacustrine sediments from the southern periphery of the Fergana Basin (Bazhenov et al., 1993) showed a declination much more rotated than that in Oligocene–Miocene rocks from the same locality (Thomas et al., 1993). In this particular area, Triassic rocks are overlain with major angular unconformity by Lower Jurassic strata; in contrast, no noticeable unconformities are found in the Lower Jurassic to Oligocene section. Taking all paleomagnetic and geological data into account, we infer that the observed rotations of Triassic rocks probably occurred in the Early Jurassic.

No oceans existed in Central Asia in the post-Early Permian, and hence, by that time, the Tien Shan had already been surrounded everywhere by continental crust. If this fold belt, about 2500 km long, was rotated as a rigid body, there should be clear signs of compression and extension. Even if the rotation was close to the values from the marginal parts of the belt, i.e., about 20° (localities D, H, L–O), and the rotation pole is in the center of the belt, the corresponding compression at its eastern and extension at its western termination will amount to about 500 km. Such a movement also leaves the main part of the observed rotations unaccounted for, whereas a rotation through a larger angle would lead to even more pronounced compensation structures, which are not observed. Also, a large post-Early Permian rotation should lead to a noticeable skewness of a flattening-versus-longitude plot, which is not the case (Fig. 12). Also, the fold belt cannot be divided into a few large blocks which rotated independently, as such a procedure will inevitably lead to great distortion of the well-established pre-Permian tectonic fabric. Moreover, there appears to be a systematic increase in rotations from the fold

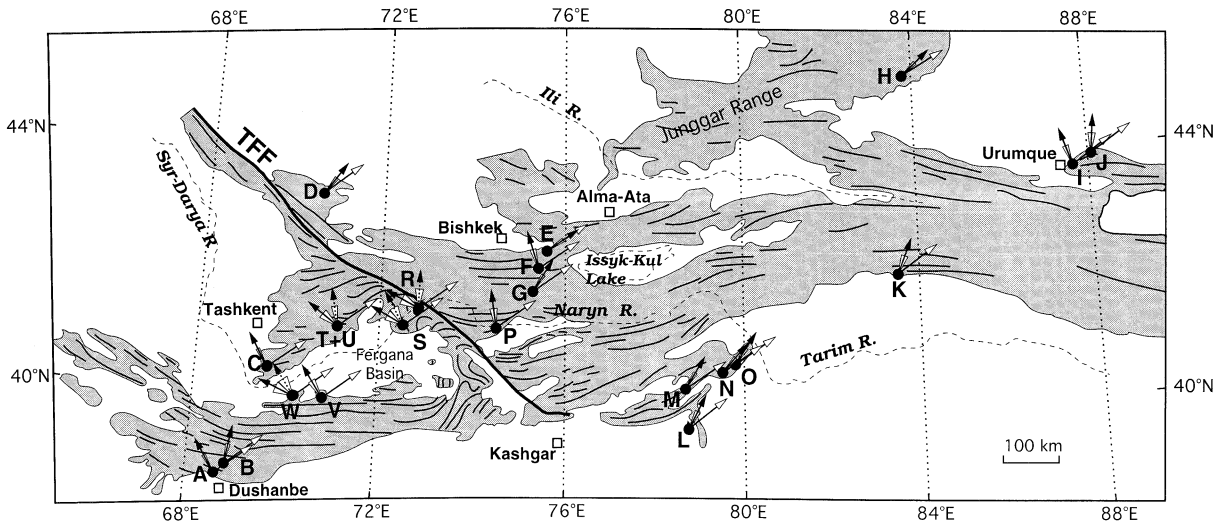


Fig. 13. The axes of late Paleozoic folds in the Tien Shan (shaded) and paleomagnetic declinations (see Table 7 for numerical values). Open arrowheads are reference declinations; solid arrowheads with solid shafts are observed declinations with associated confidence limits. For declinations of secondary components or primary components from the youngest rocks at localities R, S, T + U and W, the shafts are dotted. Confidence limits shown incorporate the confidence limits of both observed and reference declinations as in Table 7.

belt margins inward (Fig. 13), which is difficult to account for by rigid-body rotations. Thus any post-Early Permian large-scale rigid-body rotation of the Tien Shan should be rejected.

Thus the observed rotations are due to a distributed deformation of the fold belt, for instance, in book-shelf fashion (Freund, 1970). Such rotations do not lead to a large-scale disruption of the pre-existing tectonic pattern and can account for spatial variations in rotation angles. Distributed rotations have to lead to certain structural patterns which have so far been reported only from the northwestern part of the Central Tien Shan (Kiselev and Korolev, 1964). On the other hand, there may be several strike-slip faults parallel to the fold belt margins; such sinistral strike-slip associated horizontal flexures were described inside the fold belt (Mikolaichuk et al., 1995) and on the boundary of the Tien Shan and Tarim massif (Biske, 1995). In this case, the dimensions of rotated domains can be rather small. It should be noted that a simple fault system is to be expected if a more or less homogeneous matter is deformed. It is clearly not the case in the Tien Shan which consists of strongly deformed domains with a well-developed pre-Permian fault system.

We conclude that the area of large counterclock-

wise rotations in the Tien Shan is a shear zone about 300 km wide which stretches for about 2500 km along the belt. Permian declinations outside the Tien Shan belt *sensu stricto* (loc. D–E, H, L–O) indicate much smaller CCW rotations than those from the belt itself (Table 7, Fig. 13). This finding may suggest that the Tien Shan frame, including South Kazakhstan, the Junggar Range and Tarim, was also affected by strike-slip motions but of lesser magnitude than within the fold belt itself.

Good agreement of Permian declinations from South Tarim (Gilder et al., 1996) with those from North Tarim (Table 7), however, poses a problem. Gilder et al. (1996) assumed that Tarim as a rigid block rotated counterclockwise with respect to Eurasia. This interpretation, however, disagrees with geological data (Burtman, 1997). The southern part of the Tien Shan to the south from the Turkestan suture (Fig. 1b) consists of Paleozoic rocks on the Tarim basement. These rocks are represented by shelf sediments of the Tarim continental margin and had never been separated from Tarim *sensu stricto* by an ocean. All oceans in the Tien Shan were closed in the Late Carboniferous, and the Tarim massif had already been welded to the Kazakh–Kyrgyz sialic block in the Permian.

7. Alkali magmatism and the Permian stress field of the Tien Shan

Additional constraints on formation and age of the Tien Shan shear zone can be derived from spatial distribution and intensity of alkali magmatism (Fig. 14) which is regarded as an indicator of extension in the earth crust.

West Tien Shan. Numerous alkali intrusions of the Alay Range (5; the numbers correspond to those in Fig. 14) can be divided into three complexes. The Alay complex is distributed along the range crest and comprises alkali and nepheline syenites of the first phase and granosyenites, alkali granites, syenites and quartz–syenites of the second phase. This complex cuts various formations, up to Lower Permian ones. The Zardaly complex on the northern slope of the Alay Range comprises gabbro and monzonites of the first phase, alkali syenites, monzonites and essexites of the second phase and nepheline syenites of the third phase. The youngest rocks cut by the Zardaly complex are of Late Carboniferous age. Lastly, the Kichik–Alay complex in the eastern part of the Alay Range consists of granodiorites, syenite-diorites and

monzonites intruded into Lower Permian rocks (Ges et al., 1982).

The number and dimensions of alkali intrusions are considerably reduced to the west and southwest of the Alay Range. Small alkali intrusions are known from the Zeravshan (1), Hissar (2), Karategin (3), and Turkestan (4) Ranges. Trachyandesites, trachybasalts and their tuffs among Lower Permian acid volcanics and sediments are also found on the southern slope of the Hissar Range (Masumov, 1994).

To the north, a Permian volcanic series more than 5000 m thick is widespread in the Kurama (6) and Chatkal (7) Ranges. Trachybasalts, trachyandesites, trachytes, trachylyparites, trachydites and their tuffs intercalate with acid and intermediate volcanics. The alkali rocks account for 50% and 80% in the lower and middle parts of the series, respectively; their amount is reduced in the upper part. Asselian foraminifera from the lower part of the series, Permian vertebrates and plants from its middle part and Late Permian–Early Triassic plants from its top were recovered (Tulyaganov et al., 1984). Subvolcanic bodies and multiphase alkali intrusions associated with lava are mainly represented by monzonites and syenites.

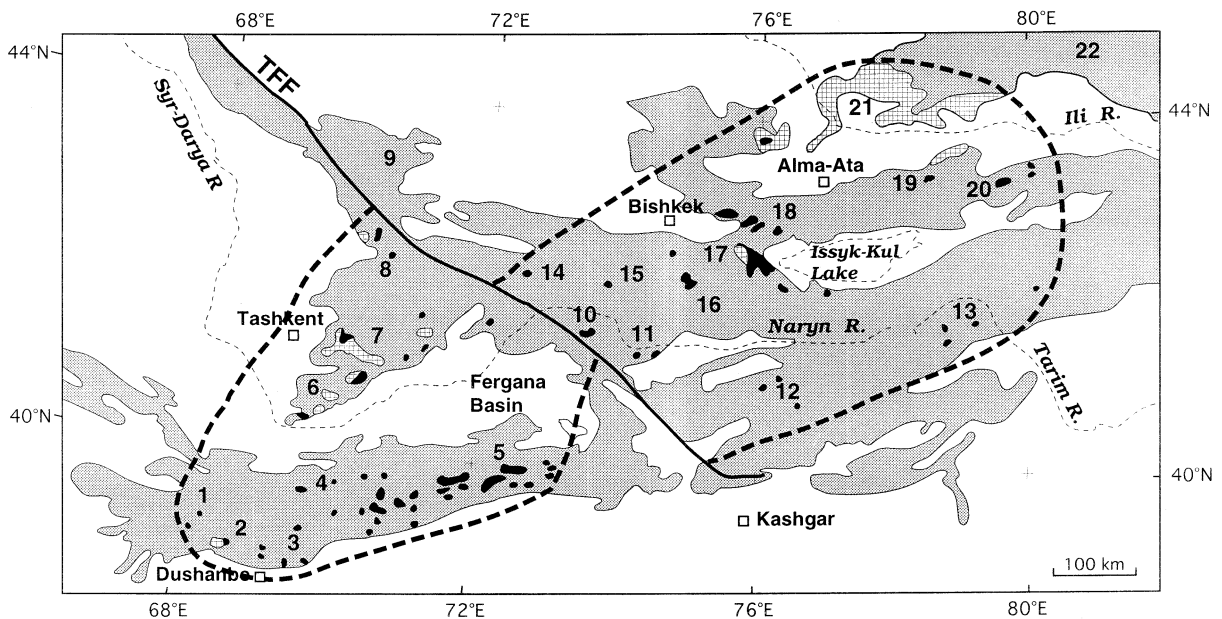


Fig. 14. Distribution of Permian alkali intrusions (black) and lava (cross-hatched) in the Tien Shan (shaded). Thick dashed line limits the area of alkali magmatism. Paleozoic rocks are shaded. TFF = Talas–Fergana Fault.

A lava series including a considerable amount of trachyandesites and trachybasalts is known further to the north in the western foothills of the Talas Range (8) (Klishevich, 1992). A Permian age of these volcanics is deduced from pollen and spores (Afonichev and Vlasov, 1984).

Central Tien Shan. In the eastern part of the Talas Range (14), the Permian multiphase Kurgan complex of alkali small intrusions and dikes is known (Ges et al., 1982), whereas no alkali rocks were found in the Lesser Karatau Range (9) further to the north.

To the south, the Shamator alkali magmatic complex in the Takhtalyk (10) and Akshyryak (11) Ranges comprises essexites and monzonites of the first phase and syenites of the second phase. Monzonites intruded into Upper Carboniferous rocks in the Akshyryak Range. K–Ar data on biotite point to a Permian age of this complex (Ges et al., 1982).

The Ortotokoy intrusive complex in the Susamyr (15), Jungol (16) and Kyrgyz (17) Ranges consists of first- and second-phase syenites and nepheline syenites, third-phase syenite-diorites and fourth-phase granosyenites which cut Upper Carboniferous sediments (Ges et al., 1982). Trachybasalts, trachyandesites and trachytes intercalate with acid and intermediate volcanics in the Kungey (18), Zaili (19) and the eastern part of the Kyrgyz (17) Ranges (Belgovsky et al., 1982). Pollen and spores of Permian affinity were found in the Kyrgyz Range (Masumov, 1994). This volcano-sedimentary series is cut by monzonites, syenite-diorites and granosyenites of the two-phase Kokmoynok complex (Ges et al., 1982).

An alkali intrusive complex consisting of granosyenites, syenites, syenite-diorites and monzonites cuts Lower Permian deposits in the Ketmen Range (20) further to the east. Rare trachyandesites were met in a thick volcano-sedimentary series with Permian plants in the western piedmont of the Borokhoro Range (21) north of the Ili River (Afonichev and Vlasov, 1984). No late Paleozoic alkali rocks altogether were found in the Junggar Range (22) further to the northeast.

The Surteke intrusive complex in the Atbashi (12) and Kokshaal (13) Ranges comprises essexites, monzonites, shonkinites and syenites; four phases were recognized in the Atbashi Range (Burov et al., 1965). The youngest rocks cut by the Surteke

complex are of Late Carboniferous–Early Permian age.

No alkali rocks are known in the East Tien Shan, except for small bodies of alkali gabbro of presumably Cenozoic age (Chen, 1985) in the southwestern part of this region.

Thus, Permian alkali intrusions and lava are confined to the western and central parts of the Tien Shan fold belt (Fig. 14). In contrast, this type of magmatism is unknown both westward, in the Kysyl Kum Desert, and eastward, in the East Tien Shan. The alkali magmatic activity is centered on the Alay, Chatkal and Kurama Ranges, gradually diminishes northward and disappears altogether in the Karatau (9) and Junggar (22) Ranges. The southern boundary of the Permian alkali province is the northern boundaries of the Tarim and Kara Kum blocks and Pamirs. Accumulation of alkali rocks spanned a considerable time as evidenced by thick lava sequences and multi-phase intrusions. Unfortunately, available stratigraphic data and radiometric ages do not allow to either better constrain the age of alkali magmatism or determine its duration.

We come to the conclusion that a wide extension province existed in the West and Central Tien Shan in the late Paleozoic. Judging by magmatism intensity, this extension was likely to be largest in the eastern part of the West Tien Shan (Fig. 14). This zone was probably initiated in the Late Carboniferous as alkali rocks are common among volcanics of this age too. Usually, the extension within a shear zone is marked by formation of pull-apart basins. We assume that the Tien Shan alkali province replaced pull-apart basins. The magnitude of extension was rather limited. On the other hand, there were probably several small basins where thick piles of either volcanics or redbeds or both accumulated in the West Tien Shan in the Permian. Note also that the largest counterclockwise rotations are found within the same province.

8. Late Paleozoic–early Mesozoic deformation of the Tien Shan

Deformation in the Tien Shan started in the Late Carboniferous when the oceanic basins which had separated the Kazakh–Kyrgyz, Alay–Tarim and Kara

Kum sialic blocks were closed. The collided blocks were deformed, and several stages of deformation, D1 to D4, are recognized (Burtman, 1975, 1980, 1984).

D1 stage. During the closure of the Turkestan Ocean, the collision of the Kazakh–Kyrgyz and Alay–Tarim blocks (Fig. 1b) led to overthrusting, mostly in the Moscovian and, locally, until the Early Permian. Recumbent folds F1 were formed in the nappes during overthrusting.

D2 stage. Nappes and autochthon were deformed into F2 folds with conjugated thrusts and reverse faults in the Late Carboniferous–Early Permian (Fig. 15). F2 folds are mostly parallel to the suture of the Turkestan Ocean and F1 folds. This implies that the continuing convergence of the Kazakh–Kyrgyz and Alay–Tarim blocks was nearly orthogonal.

D3 stage. In the Early Permian, the F2 structures were deformed into sinistral horizontal flexure (Fergana flexure) thus marking a transition from compression to strike-slip conditions (Fig. 15). The connecting limb of this flexure was rotated counterclockwise. Paleomagnetic results on Middle to Upper Carboniferous rocks appear to imply a post-Carboniferous oroclinal bending of the Fergana flexure (Klishevich et al., 1986, 1989). These data, however, are based on low-temperature blanket cleaning and are not confirmed by field tests, thus rendering the bending not well proven.

Mean declinations from the studied localities R and S in the northern part of the Fergana flexure are rather similar to declinations from the localities outside this structure (Table 7; Fig. 13). Since the studied formations and, hence, primary components at localities R and S are of Artinskian(?)–Ufimian age, the formation of the Fergana flexure had to be over by that time.

In the Late Carboniferous, the Kara Kum block had probably collided with the already welded together Kazakh–Kyrgyz and Alay–Tarim blocks (Fig. 16a). We connect the D3 deformation and earlier rotations with formation of the sinistral shear zone as the result of translation of the Kara Kum and Tarim along the Tien Shan. Some curvature of the shear zone probably led to different deformation in the western and eastern parts of the Tien Shan. While a broad wrench zone was formed in the west, a narrow basin filled with Permian terrigenous sediments was developing along the northern margin of the Tarim massif in the east (Fig. 16b).

D4 stage. During this stage, all older structures were cut by diagonal dextral strike-slip faults, the largest being the Talas–Fergana and Junggar Faults (Fig. 15). The Fergana flexure was compressed. The D4 faults disrupt all older structures and cut through the youngest (Kazanian) rocks of the Paleozoic succession of the Tien Shan. Also, there are two pull-apart basins conjugated with the Talas–Fergana Fault and filled with thick terrigenous coal-bearing Liasic sediments (Burtman, 1980). The later phase of rotation implied by Late Permian and Triassic declinations took place during this stage of deformation. These counterclockwise rotations indicate that the Tien Shan shear zone is sinistral. On the other hand, paleomagnetic declinations in Lower Cretaceous and

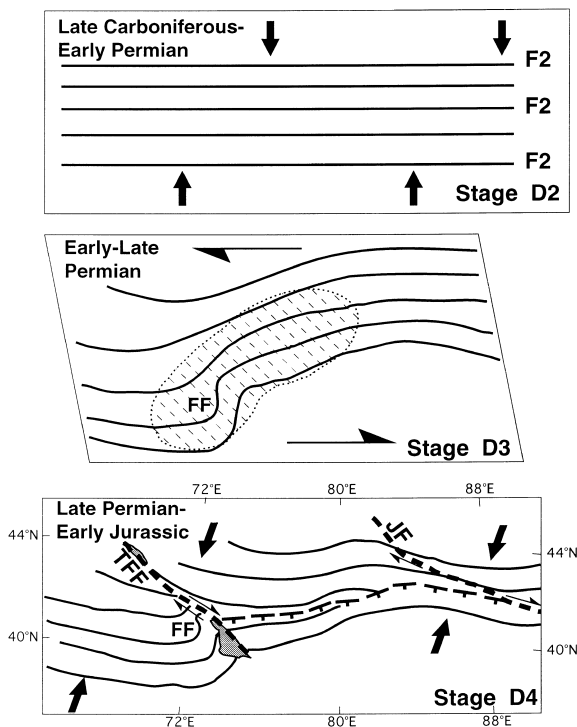


Fig. 15. A scheme of formation of the late Paleozoic structure of the Tien Shan (stages D2 to D4). F2 folds: thin solid lines; Permian alkali magmatism: dashed area; main strike-slip faults: thick dashed lines; TFF = Talas–Fergana Fault, JF = Junggar Fault; main thrusts: toothed line. Early Jurassic pull-apart basins conjugated with the Talas–Fergana Fault are shaded. FF = Fergana flexure. Large arrows denote stress field during each stage.

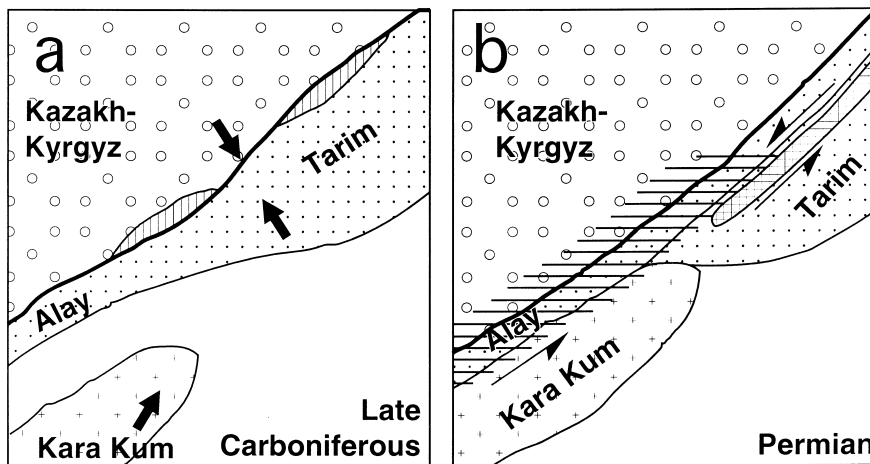


Fig. 16. Major blocks in the Tien Shan region (a) in the Late Carboniferous and (b) Permian. Vertical striping denotes small basins close to the Turkestan suture (thick solid line) where marine sedimentation lasted until the Early Permian. Horizontal striping denotes the area affected by rotations. Cross-hatched band is the Permian sedimentary basin separating the Tarim massif from its northern deformed margin (see text).

younger formations (see above) are rotated much less than the Permian and Triassic directions. Thus, D4 deformation was due to transpression with a diffuse shear component distributed over the Tien Shan and could last from the Late Permian until the Early Jurassic.

It is worth adding that the structural units were considered rigid and rotated according to paleomagnetic declinations in most previously presented palinspastic reconstructions of the composite Eurasian continent (e.g., Enkin et al., 1992). Such an approach, however, leads to appearance of inter-block gaps which are difficult to reconcile with geological data. Our results imply that block rigidity may be exaggerated, and observed rotations of paleomagnetic vectors may result from ductile deformation of vast regions comprising both fold belts and presumably rigid units.

9. Conclusions

The above-presented new and previously published Permian inclinations from the Tien Shan and adjacent regions agree well with the reference directions for the East European platform. This finding indicates that all tectonic units, including those of the Urals and Kazakhstan, had already been welded together in the middle Permian. In contrast, Permian

declinations from the Tien Shan are rotated counterclockwise through varying angles. A rigid-body rotation of the Tien Shan is rejected; instead, a 2500 km long and 300 km wide shear zone is hypothesized in this region. Two rotations are recognized. The earlier rotation of the Artinskian–Ufimian age is established in the western part of the Tien Shan and is connected with oblique collision of the Kara Kum microcontinent with the Eurasian landmass. The later rotation which encompassed the entire Tien Shan took place between the Late Permian and Early Jurassic.

The proposed scenario should be further tested by studies of Permian and Triassic rocks in and around the Tien Shan. An expanded data set will help to better recognize the rotations of rigid blocks from distributed deformation and thus improve our understanding of the Asian tectonic evolution.

Acknowledgements

Thanks are due to Jean-Pascal Cogné, Randy Enkin and Stanislav Shipunov for the software used in this study and to Nina Dvorova for assistance in the laboratory. We thank Yan Chen, Rob Van der Voo and the anonymous reviewers for helpful comments and suggestions. This work was supported by grants M45000 and M45300 from the Interna-

tional Science Foundation and grants 97-05-65084 and 97-05-64124 from the Russian Foundation of Fundamental Studies.

References

- Afonichev, N.A., Vlasov, N.G., 1984. Explanatory notes to geological map of Kazakhstan and Middle Asia (1 : 1,500,000) (in Russian). VSEGEI, Leningrad, 234 pp.
- Akhmejanov, M.A., Baratov, R.B., Bakirov, A.B., Borisov, O.M., Korolev, V.G., Mirkhojaev, I.M., Fuzaylov, I.A., Abdullaev, R.N., Bazarbaev, E.R., Budanov, V.I., Budanova, K.T., Kiselev, V.V., Masumova, R.A., 1982. Precambrian of Central Asia (in Russian). Nauka, Leningrad, 264 pp.
- Audibert, M., Bazhenov, M.L., 1992. Permian paleomagnetism of the North Tien Shan: tectonic implications. *Tectonics* 11, 1057–1070.
- Bai, Y., Chen, G., Sun, Q., Li, Y., Dong, Y., Sun, D., 1987. Paleozoic polar wander path for the Tarim platform and its tectonic significance. *Tectonophysics* 139, 145–153.
- Bakirov, A.B., Biske, G.S., Burtman, V.S., Klishevich, V.L., 1984. The oldest rocks of the Turkestan ocean. In: Bakirov, A.B., Burtman, V.S. (Eds.), *Tectonics of the Tien Shan Variscides*. 27th Int. Geol. Congr., Moscow, Guidebook for excursion 032 in the Kyrgyz Republic. Frunze, Kyrgyzstan, pp. 55–59.
- Bazhenov, M.L., 1993. Cretaceous paleomagnetism of the Fergana basin and adjacent ranges, central Asia: tectonic implications. *Tectonophysics* 221, 251–267.
- Bazhenov, M.L., Chauvin, A., Audibert, M., Levashova, N.M., 1993. Permian and Triassic paleomagnetism of the south-west Tien Shan: the timing and mode of tectonic rotations. *Earth Planet. Sci. Lett.* 118, 195–212.
- Bazhenov, M.L., Burtman, V.S., Cobbold, P.R., Perroud, H., Sadybokasov, I., Thomas, J.-C., Chauvin, A., 1994a. Paleomagnetism of Tertiary deposits and Alpine kinematics of the Tien Shan. *Geotectonics* 27, 492–504.
- Bazhenov, M.L., Perroud, H., Chauvin, A., Burtman, V.S., Thomas, J.-C., 1994b. Paleomagnetism of Cretaceous red beds from Tadjikistan and Cenozoic deformation due to India–Eurasia collision. *Earth Planet. Sci. Lett.* 124, 1–18.
- Bazhenov, M.L., Klishevich, V.L., Tselmovich, V.A., 1995. Paleomagnetism of Permian red beds from south Kazakhstan: DRM inclination error or CRM shallowed directions? *Geophys. J. Int.* 120, 445–452.
- Belgovsky, G.L., 1972. The Permian system (in Russian). In: Pomazkov, K.D. (Ed.), *Kyrgyzskaya SSR*, v. 25-1. Nedra, Moscow, pp. 190–200.
- Belgovsky, G.L., Biske, G.L., Vlasov, N.G., Voytovich, I.I., Kotelnikov, V.I., Khristov, V.I., Yagovkin, A.V., 1982. The Permian system (in Russian). In: Osmonbetov, K.O., Knauf, V.I., Korolev, V.G. (Eds.), *Stratified and Intrusive Formations of Kyrgyzia*. Ilim, Frunze, 1, pp. 314–324.
- Biske, G.S., 1995. Late Paleozoic collision of the Tarim and Kyrgyz–Kazakh paleocontinents. *Geotectonics* 29, 26–34.
- Bolshakov, A.S., Solodovnikov, G.M., Vinogradov, Y.K., 1989. Paleointensity of Early Permian geomagnetic field (in Russian). *Izv. Akad. Nauk SSSR, Ser. Fizika Zemli* 7, 70–77.
- Burov, V.G., Purkin, M.M., Khristov, E.V., Khristova, M.P., 1965. Surteke calc-alkaline intrusion (in Russian). *Reports of Kyrgyz Branch of All-Union Mineralogical Society* 5, pp. 39–49.
- Burtman, V.S., 1975. The structural geology of Variscan Tien Shan, USSR. *Am. J. Sci.* 275, 157–186.
- Burtman, V.S., 1980. Faults of Middle Asia. *Am. J. Sci.* 280, 725–744.
- Burtman, V.S., 1984. Structural evolution of the Tien Shan Variscides. In: Bakirov, A.B., Burtman, V.S. (Eds.), *Tectonics of the Tien Shan Variscides*. 27th Int. Geol. Congr., Moscow, Guidebook for excursion 032 in the Kyrgyz Republic. Frunze, Kyrgyzstan, pp. 36–43.
- Burtman, V.S., 1997. Kyrgyz Republic. In: Moores, E.M., Fairbridge, R.W. (Eds.), *Encyclopedia of European and Asian Regional Geology*. Chapman and Hall, London, pp. 483–492.
- Chen, Y., Cogné, J.-P., Courtillot, V., Avouac, J.-P., Tapponnier, G., Wang, M., Bai, H., You, M., Li, C., Wei, C., Buffetaut, E., 1991. Paleomagnetic study of Mesozoic continental sediments along the Northern Tien Shan (China) and heterogeneous strain in Central Asia. *J. Geophys. Res.* 96 (B3), 4065–4082.
- Chen, Y., Cogné, J.-P., Courtillot, V., 1992. New Cretaceous paleomagnetic results from the Tarim basin, Northwestern China. *Earth Planet. Sci. Lett.* 114, 17–38.
- Chen, Z., 1985. Geological map of Xinjiang Uygur Autonomous Region (China), scale 1 : 2,000,000, with explanatory notes. Beijing, 82 pp.
- Cobbold, P.R., Davy, P., 1988. Indentation tectonics in nature and experiment, 2. Central Asia. *Bull. Geol. Inst. Univ. Uppsala*, N.S. 14, 143–162.
- Cogné, J.-P., Chen, Y., Courtillot, V., Rocher, F., Wang, G., Bai, M., You, H., 1995. A paleomagnetic study of Mesozoic sediments from the Junggar and Turfan basins, northwestern China. *Earth Planet. Sci. Lett.* 133, 353–366.
- Demarest, H.H., 1983. Error analysis for the determination of tectonic rotation from paleomagnetic data. *J. Geophys. Res.* 88, 4321–4328.
- Enkin, R.J., Yang, Z., Chen, Y., Courtillot, V., 1992. Paleomagnetic constraints on the geodynamic history of the major blocks of China from the Permian to the Present. *J. Geophys. Res.* 97, 13953–13989.
- Freund, R., 1970. Rotation of strike-slip faults in Sistan, Southeast Iran. *J. Geol.* 2, 188–201.
- Ges, M.D., Garetskaya, E.N., Izraileva, R.M., Leskov, S.A., 1982. Permian intrusive rocks (in Russian). In: Osmonbetov, K.O., Knauf, V.I., Korolev, V.G. (Eds.), *Stratified and Intrusive Formations of Kyrgyzia*. Ilim, Frunze, 2, pp. 128–181.
- Gilder, S.A., Zhao, X., Coe, R.S., Meng, Z., Courtillot, V., Besse, J., 1996. Paleomagnetism and tectonics of the southern Tarim basin, northwest China. *J. Geophys. Res.* 101, 22015–22032.
- Khramov, A.N., Goncharov, G.I., Komissarova, R.A., Pisarevsky, S.A., Pogarskaya, I.A., Rzhovsky, Y.S., Rodionov, V.P., Slautsitais, I.P., 1982. Paleomagnetology (in Russian). Nedra, Leningrad, 312 pp.
- Kirschvink, J.L., 1980. The least-square line and plane and the

- analysis of palaeomagnetic data. *Geophys. J.R. Astron. Soc.* 62, 699–718.
- Kiselev, V.V., Korolev, V.G., 1964. Strike-slips and rotational structures in the western part of the Kyrgyz Range (in Russian). *Reports on Geology of the Tien Shan* 4, pp. 147–151.
- Klishevich, V.L., 1992. Explanatory notes to Geological map of the USSR (1 : 100,000), sheet K-42,43 (in Russian). VSEGEI, St. Petersburg, 134 pp.
- Klishevich, V.L., Klishevich, I.A., Rzhovsky, Y.S., Khramov, A.N., 1986. On the Fergana sigmoidal structure (in Russian). *Dokl. Akad. Nauk SSSR* 286, 402–405.
- Klishevich, V.L., Rzhovsky, Y.S., Khramov, A.N., Talashmanov, Y.A., Krylova, T.N., 1989. Late Variscan deformations of the Fergana part of the Tien Shan (in Russian). *Reports of Leningrad University*, 1 (7), pp. 3–10.
- Kumpan, A.S., Rusinov, B.S., Sholpo, L.E., 1968. Paleomagnetic investigations in Central Kazakhstan (in Russian). *Izv. Akad. Nauk SSSR, Phys. Earth* 11, 96–103.
- Li, Y.P., McWilliams, M., Cox, A., Sharps, R., Li, Y.A., Gao, Z.J., Zhang, Z.K., Zhai, Y.J., 1988a. Late Permian paleomagnetic pole from dikes of the Tarim craton. *Geology* 16, 275–278.
- Li, Y.P., Zhang, Z.K., McWilliams, M., Sharps, R., Zhai, Y.J., Li, Y.A., Li, Q., Cox, A., 1988b. Mesozoic paleomagnetic results of the Tarim craton: Tertiary relative motion between China and Siberia? *Geophys. Res. Lett.* 15, 217–220.
- Mardia, K.V., 1972. *Statistics of Directional Data*. Academic Press, London, 357 pp.
- Masumov, A.S., 1994. Late Paleozoic of the Central and West Tien Shan (in Russian). Dr. Sci. thesis, MGU, Moscow, 50 pp.
- McElhinny, M.W., 1964. Statistical significance of the fold test in palaeomagnetism. *Geophys. J.R. Astron. Soc.* 8, 338–340.
- McFadden, P.L., Jones, D.L., 1981. The fold test in palaeomagnetism. *Geophys. J.R. Astron. Soc.* 67, 53–58.
- McFadden, P.L., Ma, X.H., McElhinny, M.H., Zhang, Z.K., 1988. Permo–Triassic magnetostratigraphy in China: northern Tarim. *Earth Planet. Sci. Lett.* 87, 152–160.
- Mikolaichuk, A.V., Kotov, V.V., Kuzikov, S.I., 1995. Structural position of the Malyi Naryn metamorphic complex and the boundary between the North and Median Tien Shan (in Russian). *Geotectonics* 2, 75–85.
- Molnar, P., Tapponnier, P., 1975. Cenozoic tectonics of Asia: effects of a continental collision. *Science* 189, 419–426.
- Nie, S.Y., Rowley, D.B., Van der Voo, R., Li, M.S., 1993. Paleomagnetism of Late Paleozoic rocks in the Tianshan, northwestern China. *Tectonics* 12, 568–579.
- Sharps, R., McWilliams, M., Li, Y.P., Cox, A., Zhang, Z., Zhai, Y., Gao, Z., Li, Y.A., Li, Q., 1989. Lower Permian paleomagnetism of the Tarim block, northwestern China. *Earth Planet. Sci. Lett.* 92, 275–291.
- Sharps, R., Li, Y.P., McWilliams, M., Li, Y., 1992. Paleomagnetic investigation of Upper Permian sediments in the South Junggar Basin, China. *J. Geophys. Res.* 97, 1753–1765.
- Thomas, J.-Ch., Perroud, H., Cobbold, P.R., Bazhenov, M.L., Burtman, V.S., Chauvin, A., Sadybokasov, E., 1993. A paleomagnetic study of Tertiary formations from the Kyrgyz Tien Shan and its tectonic implications. *J. Geophys. Res.* 98, 9571–9589.
- Tulyaganov, H.T., Yudalevich, Z.A., Korzhaev, V.P., Kim, O.I., Yaskovich, B.V., Kozlov, S.A., Ponikalenko, I.A., 1984. Explanatory Notes to the Map of Magmatic Complexes of the Uzbek SSR (in Russian). FAN, Tashkent, 345 pp.
- Van der Voo, R., 1993. *Paleomagnetism of the Atlantic, Tethys and Iapetus Oceans*. Cambridge University Press, Cambridge, 411 pp.
- Zhao, X., Coe, R.S., Zhou, Y., Wu, H., Wang, J., 1990. New paleomagnetic results from northern China: collision and suturing with Siberia and Kazakhstan. *Tectonophysics* 181, 43–81.